Electronic Structure of Semiconductor Superlattices in Strong Magnetic Fields

Contents

Chapter 1

Introduction

Recent experiments performed on a two–dimensional modulated electron gas (or a system of coupled quantum wires) showed huge magnetoresistance oscillations [4]. In this work we would like to present a theoretical model describing this phenomenon, i.e. we will find out how does the system conductivity depend on magnetic field applied perpendicular to the plane of the system. We will use a full quantum mechanical calculation rather than the standardly used semiclassical theory. Heading for this aim we will find out that the system can undergo substantial changes when the magnetic field is increased. This is a phenomenon which cannot be described by a semiclassical model.

Further we will focus on three–dimensional superlattices or in other words coupled two–dimensional electron systems (2DES). Compared to the previous case the system has now another degree of freedom, namely the field direction. If the field is perpendicular to the planes of the 2DES the problem can be solved analytically, we mean the density of states in the tight–binding approximation now. The semiclassical prediction is in a full agreement with the quantum mechanical prediction. However if the field is tilted the quantum mechanical problem to solve leads to a two–dimensional Schrödinger equation and we lose the analytical solution. If the in–plane component of the magnetic field is strong enough we will show that the dimensionality of the system changes. This is again a feature of the full quantum description only and it is not predicted by the semiclassical theory.

Modulated two dimensional systems have already been a point of interest of theoretical studies (Zhang et al. [16] or recently Manolescu et al. [11]). Both mentioned works use the one–electron approximation (as we do in this

work) and include advanced models of the electron scattering on impurities (which are reduced to the simplest possible model in this work).

Let us finish the introduction with a quick review of the structure of this work. Both Chapters 2 and 3 contain a brief comment on the semiclassical approach to the superlattice systems followed by a quantum mechanical derivation of an equation which yields the spectrum (and density of states) of the system. There is a discussion of the possible form of the results in Chapter 2 before the numerical results are presented.

As the results of two–dimensional SLs calculations could be compared to an experiment, the Chapter 2 does not stop at this point. There follows a section about the linear response theory and a section concerning the procedures necessary to link the theory and experimental data including also a discussion on the level of density of states (which is much more straightforward than the Kubo formula). Finally the comparison of theory and experiments is presented.

Chapter 2

Two–Dimensional Superlattices

2.1 Introduction

2.1.1 Description of the System

We are going to speak about a planar structure referred to as a lattice of quantum wires. We suppose that electrons can move only in the x, y-plane and that they are confined by a periodic (or quasiperiodic) potential $V = V(y)$, i.e. the motion in the x direction (along the stripes) is free. The
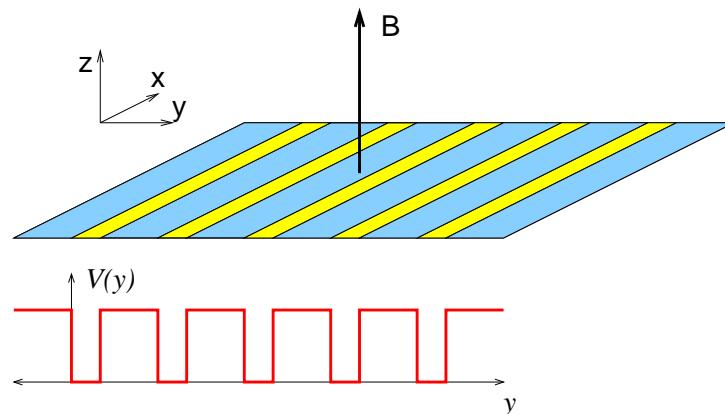

Figure 2.1: Quantum wires.

potential $V(y)$ can be either periodic from minus infinity to plus infinity or it can be composed of N (finite number of) periods (and be enclosed in an

infinitely deep well). We examine the effect of magnetic field applied in the direction perpendicular to the lattice plane (i.e. z).

2.1.2 Semiclassical Approach

The semiclassical (SC) model describing the motion of an electron in magnetic field B is based on constructing the Fermi surface for the zero magnetic field system (given the Fermi level E_F). The spectrum of such a system can be computed analytically in the tight–binding approximation

$$E(k_x, k_y) = \frac{\hbar^2}{2m_*}k_x^2 - 2|t|\cos k_y d \,.$$

Here d is the superlattice period and t is the coupling constant between two neighbouring wells in the superlattice (see section 2.2.1 and Eq. 2.11 for comments on derivation of this spectrum).

The Fermi surface $E_F = E(k_x, k_y)$ can be one of three topologically different types, see Fig. 2.2. It consists of disconnected closed ovals ($E_F < 2|t|$), it can be a pair of rippled lines ($E_F > 2|t|$) or it can be a set of just touching lens–like figures for $E_F = 2|t|$.

The SC theory states that the real space trajectories of the electron in magnetic field can be obtained by rotating the Fermi contours by 90 degrees (around the magnetic field direction) and scaling them by $\hbar/|e|B$ [1].

Furthermore the SC theory claims that only those *closed* trajectories are permitted which enclose an integer multiple of magnetic flux quanta $|e|B/h$, [1]. This is an ad hoc quantization condition similar to the one in Bohr's model of hydrogen atom. There is no quantization condition for the open trajectories[1].

Thus for $E_F < 2|t|$ the "permitted" energies (or Landau levels energies) are determined for each magnetic field. If we set E_F constant and change B, these levels are passing through E_F periodically[2] in $1/B$, which gives rise to the Shubnikov–de Haas oscillations.

---

[1]This concept is based on the idea that closed trajectories should correspond to bound states and these are known to have discrete spectra unlike the unbound states. This is however no proof of correctness but rather an indication why can the SC theory give some relevant results at all.

[2]The values of $1/B$ at which there will be a state at the Fermi level will be $1/B = (ne/h) \cdot 1/A(E_F)$, $n = 1, 2, \ldots$, where $A(E_F)$ is the area enclosed by the Fermi contour for the given E_F.

The prediction for $E_F < 2|t|$ is therefore that electrons move along closed orbits which are almost oval unless E_F is very near to $2|t|$ (then the orbits approach the critical shape, see Fig. 2.2). The system is in a two dimensional mode. If we study the magnetic field dependent conductivity of the system we find Shubnikov–de Haas oscillations. On the other hand for $E_F > 2|t|$ the electrons move almost freely in the x direction and the conductivity should exhibit no oscillations when e.g. increasing magnetic field.

Fermi contour

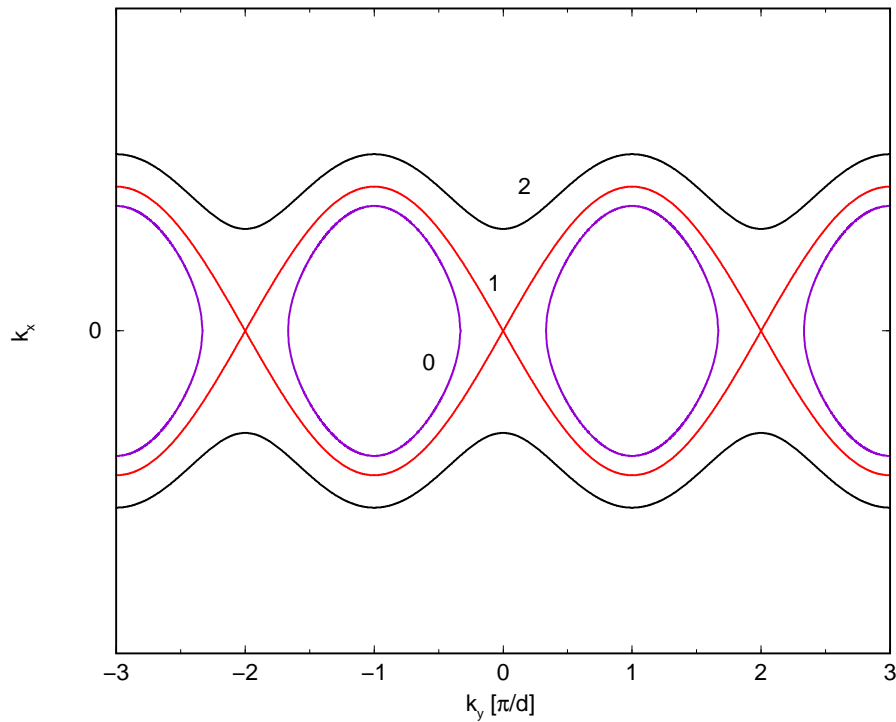Figure 2.2: Semiclassical trajectories in magnetic field. 0 – closed ($E_F < 2|t|$), 1 – critical ($E_F = 2|t|$), 2 – open ($E_F > 2|t|$).

This concept however fails to explain the following situation. Consider $E_F > 2|t|$ and "weak" magnetic field. Electrons then move on cycloidal (open) trajectories along an edge of one of the superlattice wells in the x–

direction[3]. When we increase the magnetic field so that the cyclotron radius ($m_* v/|e|B$, where $v = \sqrt{2E_F/m_*}$) becomes much smaller than the superlattice period d, only a minority of electrons located near to the edge of a well will proceed on the open cycloidal trajectories and the rest will move along circles inside wells. The system will turn into the 2D mode. The semiclassical theory however still predicts the electron to move along an open orbit. This effect is called *the breakdown of the semiclassical theory*[4]. An evidence of the semiclassical theory failure is the presence of magnetoresistivity oscillations even for $E_F > 2|t|$ which can be observed in an experiment.

So as to conclude: the disadvantage of the semiclassical theory is that it cannot reflect the qualitative changes to the system which are induced by magnetic field. On the other hand there is a separate Hamiltonian corresponding to each strength of magnetic field in the quantum mechanical approach and thus the electron states at the same Fermi energy can substantially differ at various magnetic fields.

2.2 Schrödinger Equation and Density of States

2.2.1 Quantum Mechanical Calculation

Taking the calibration of the magnetic field as $\boldsymbol{A} = (B_z y, 0, 0)$, the Hamiltonian of the system at Fig. 2.1 reads

$$\boldsymbol{H} = \frac{1}{2m_*}\left(\boldsymbol{p} - e\boldsymbol{A}\right)^2 + V(\boldsymbol{y}) = \frac{1}{2m_*}\left[-\imath\hbar\frac{\mathrm{d}}{\mathrm{d}x} + |e|B_z y\right]^2 + \frac{1}{2m_*}\boldsymbol{p}_y^2 + V(y).$$

We denote the last two terms by $\boldsymbol{H}_y$. Exploiting the translational invariance in the x direction we first make an ansatz $\Psi(x,y) = \exp(\imath k_x x)\psi(y)$ for the Schrödinger equation and get

$$\left\{\frac{1}{2m_*}\boldsymbol{p}_y^2 + \frac{1}{2m_*}\left[\hbar k_x + |e|B_z y\right]^2 + V(y)\right\}\psi(y) = E(k_x)\psi(y). \qquad (2.1)$$

---

[3]Assuming elastic rebounces at the well edge, this problem can be easily solved on the classic level.

[4]This expression was first proposed by Stark and Falicov [14] in the context of physics of metals.

This is a 1D Schrödinger equation for a particle confined by parabolical potential with periodic "ripples" superposed on it. However, we have no exact information about the form of the periodic potential $V(y)$ apart from its period d. Our idea about the potential is that it consists of a chain of quantum wells (one well per period).

We are going to solve the equation (2.1) by means of the tight-binding approximation [1]. We suppose that each well of $V(y)$ is capable of accommodating one state which is then localised in this well. Denoting the state localised in one well by $|\varphi(y - jd)\rangle$, assumption made by the tight–binding approximation is

$$\langle\varphi(y - jd)|\boldsymbol{H}_y|\varphi(y - kd)\rangle = t\delta_{jk\pm 1}, \qquad \langle\varphi(y - jd)|\varphi(y - kd)\rangle = \delta_{jk}.$$

The interpretation is that only the states in two neighbouring wells overlap considerably. Condition $\langle\varphi(y - jd)|\boldsymbol{H}_y|\varphi(y - jd)\rangle = 0$ sets only the position of the origin of the energy scale. Remaining requirements only claim that the states $|\varphi(y - jd)\rangle$ are orthonormalised.

We can be thus looking for the solution to Eq. (2.1) having the form

$$\psi(y) = \sum_{j=1}^{N} a_i\varphi(y - jd)\,. \tag{2.2}$$

Followingly we arrive to a *finite* set of linear equations for a_i (or a matrix eigenvalue problem)

$$\sum_{j=1}^{N} H_{jl}(k_x)a_j = E(k_x)a_l, \text{ where} \tag{2.3}$$

$$H_{jj} = \frac{\hbar^2}{2m_*}\left[\frac{|e|B_z}{\hbar}jd + k_x\right]^2, \quad H_{jj\pm 1} = t.$$

If we imagine N to be infinity (or large), the system described by (2.3) has to behave periodically in k_x with the period $K = d|e|B_z/\hbar$ (or quasi–periodically). We are thus interested only in solving the eigenvalue problem (2.3) within the "first Brillouin zone[5]" $(-\frac{1}{2}K, \frac{1}{2}K)$, see Fig. 2.3.

In other words: we get infinite number of (Landau) bands $E_i(k_x)$ which are K–periodic in k_x as a solution to the problem (2.3) in the limit $N \to \infty$.

---

[5]This has, however, no interpretation in terms of the geometrical periodicity of the lattice.

If we perform numerical calculations with finite N we obtain N bands which are not exactly periodic in k_x, but they are nearly periodic on the interval $(-\frac{1}{2}NK, \frac{1}{2}NK)$, the more we approach the limits of this interval the bigger is the deviation from the periodical behaviour. This fact is clearly demonstrated on Fig. 2.4 where we display $E_i(k_x)$ on the first twenty "Brillouin zones" for $N = 10$.

Setting $jd|e|B_z/\hbar = jK = k_j$ we find Eq. 2.3 formally similar to a matrix form of the Schrödinger equation in the basis of plane waves (again in the limit $N \to \infty$, see [1], Chapter "Nearly free electrons approximation")

$$\left[\frac{\hbar^2}{2m_*}(k_x - k_j)^2 - E\right] a_j + \sum_{l=-\infty}^{\infty} V_{l-j} a_l = 0, \text{ with } V_n = K \int_0^d e^{-\imath n K x} V(x) \, \mathrm{d}x \,,$$

V_n are the Fourier components of the potential V in the x direction. Comparing the Fourier series with Eq. 2.3 we can see that $V_{l-j} = t\delta_{lj\pm1}$, i.e. $V_{\pm1} = t$ and $V_{\pm n} = 0$ for $n = 0, 2, 3, 4, \ldots$. That means that $V(x) = t[\exp(\imath K x) + \exp(-\imath K x)] = 2t\cos Kx$ and consequently *if N were infinity* then the Eq. 2.3 is equivalent to the Mathieu equation [7]:

$$\left\{-\frac{\hbar^2}{2m_*}\frac{\mathrm{d}^2}{\mathrm{d}x^2} + 2|t|\cos Kx\right\} \mathrm{e}^{ik_x x} u(x) = E\mathrm{e}^{ik_x x} u(x) \,. \qquad (2.4)$$

This can also be understood as a 1D Schrödinger equation $\boldsymbol{H}\chi = E\chi$ (for $\chi(x) = \exp(\imath k_x x)u(x)$) for a fictive particle in a cosine potential. Although we do not see a straightforward relation between χ and ψ (from Eq. 2.1) we know that the spectra have Eq. 2.4 and Eq. 2.1 have to be the same.
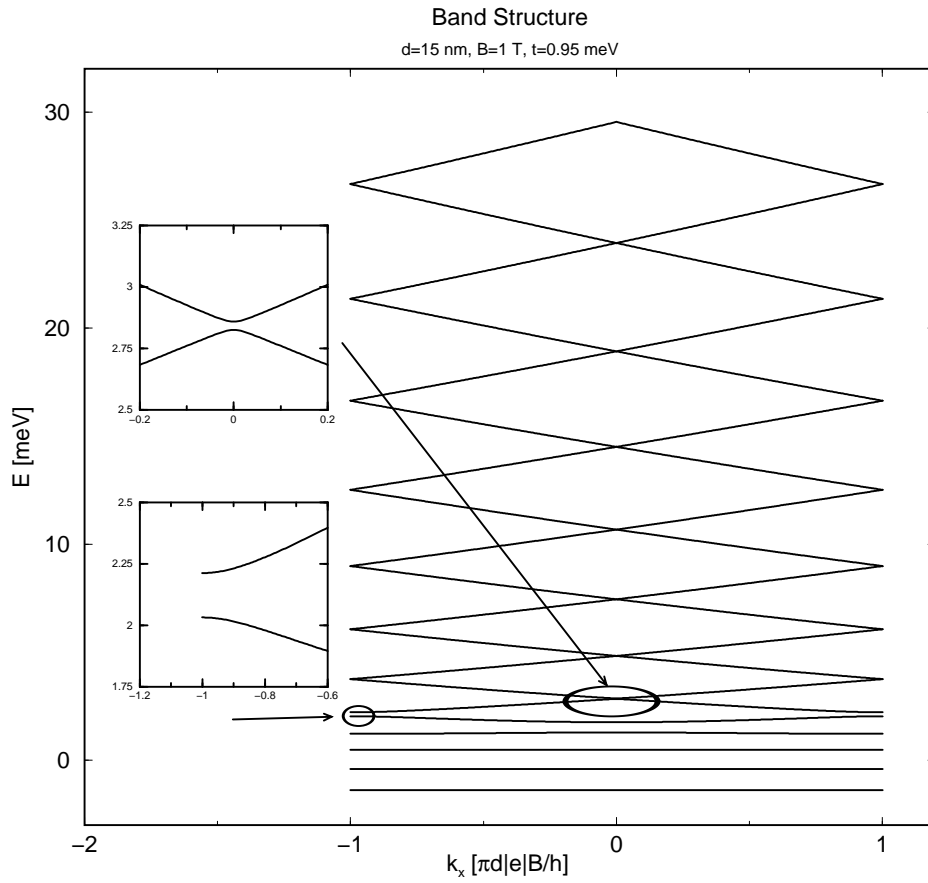
Figure 2.3: One of the results of the matrix diagonalization problem (Eq. 2.3): first 20 eigenvalues are displayed ($N = 40$) for k_x running through the first Brillouin zone $\left(-\frac{1}{2}K, \frac{1}{2}K\right)$.

Band Structure – repeated zone scheme

d=15 nm, t=0.95 meV, N=10
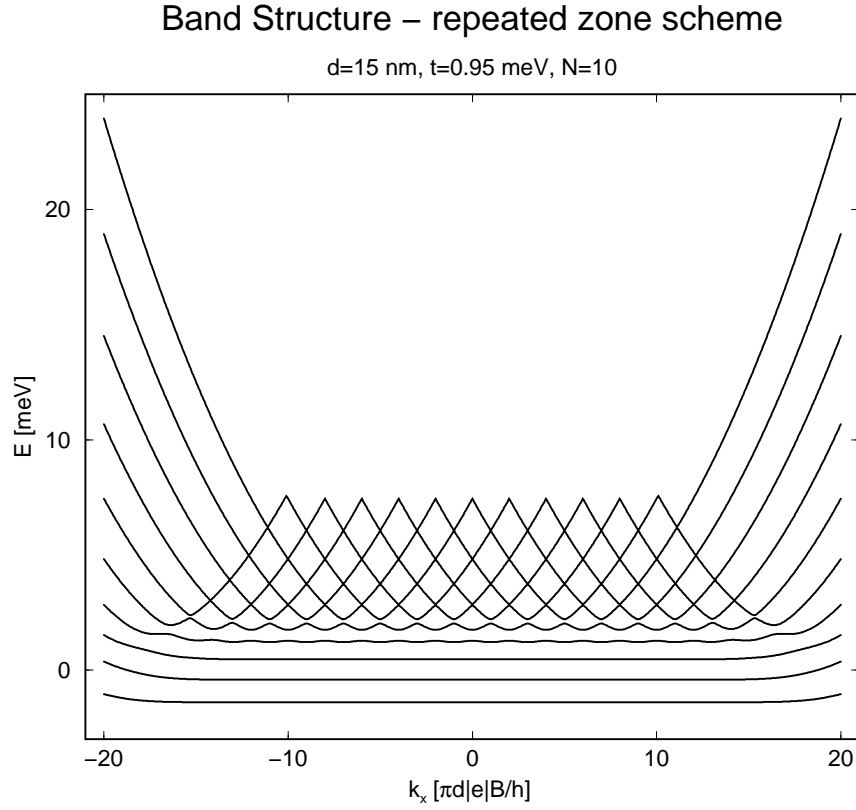
Figure 2.4: Demonstration of the k_x-quasi–periodicity of the spectrum. The potential $V(y)$ consists of $N = 10$ periods and we plot first 20 Brillouin zones (according to the scaling of the horizontal axis, the nth Brillouin zone is located at $(-n, n) \setminus (-n + 1, n - 1)$). It is however well visible that the bands are almost periodic up to the 10th Brillouin zone.

Density of States

The standard definition of density of states (DOS) at a given energy level E_F for any dimensionality n is

$$g(E_F) = \frac{1}{(2\pi)^n} \int_{E(k)=E_F} \mathrm{d}k = \frac{1}{(2\pi)^n} \int_\Omega \mathrm{d}k\, \delta\Big(E - E(k)\Big) \qquad (2.5)$$

whereas Ω denotes the complete k–space. In our case, the k–space is one dimensional and thus the second expression can be rewritten as

$$g(E_F) = \frac{1}{(2\pi)} \sum_{k,\, E_i(k)=E_F} \left| \frac{\mathrm{d}E}{\mathrm{d}k} \right|^{-1} . \qquad (2.6)$$

However, this formula causes serious inaccuracies for flat bands (i.e. when $\mathrm{d}E/\mathrm{d}k \approx 0$ for all $k \in \left(-\frac{1}{2}K, \frac{1}{2}K\right)$) in numerical calculations. It is much more suitable to use the relation

$$g(E_F) = d \cdot \frac{\partial N}{\partial E}(E_F), \qquad N(E_F) = \frac{1}{d} \int_{-\infty}^{E_F} \mathrm{d}E\, g(E) . \qquad (2.7)$$

N is the total number of states having energy under the Fermi level E_F. This quantity can be determined with a good accuracy employing the fact that the total number of states per Landau band is $|e|B/h$ (see Appendix B).

2.2.2   Structure of the Energy Bands

The equation easiest to solve numerically is (2.3), however the structure of the spectrum is best to see from Eq. 2.4. We will now try to get a better insight into the problem which will help us to understand the numerical results better.

Let us investigate the eigenfunctions of Eq. 2.4; we will denote the cosine potential in Eq. 2.4 by $W(x)$. If $E > 2|t|$ the eigenstates of Eq. 2.4 should correspond to almost free particles, which percept $W(x)$ only as a weak perturbation.

According to the results of the almost–free–electrons *approximation* [1] we suppose that $E(k_x)$ are near to parabolas, which are deformed in the vicinity of the first Brillouin zone boundaries $k_x = \pm\frac{1}{2}K$ (gaps open here).

Next we focus on the states corresponding to energies near to a minimum of $W(x)$. Imagine there is an infinitely high barrier between two minima of

the cosine potential, i.e. no tunnelling between two neighbouring wells of $W(x)$ is possible (note that this has nothing to do with the value of t). Then there would appear bound states in each well of $W(x)$ the energy of which would be independent on k_x; thus the spectrum would consist of flat bands.

Although this is not our case, the states with energies near to the bottom of a well in $W(x)$ are sufficiently separated from the neighbouring wells and the k_x dependence of their energies will thus be weak. We expect almost flat bands in this range of energies. Furthermore, these energies can be computed approximatelly as the ones of bound states in a single well of $W(x)$ (which is not surrounded by other wells).

Thus when $E \ll 2|t|$, we can suppose that the wavefunction is localised at $|x| \ll \pi/K$. Expanding the potential in Eq. (2.4) around its minimum[6] (suppose that $t < 0$)

$$2t \cos Kx = -2|t| + \frac{|t|d^2 e^2 B_z^2}{\hbar^2}x^2 + O(x^4)$$

and comparing it to the linear harmonic oscillator problem with the potential $\frac{1}{2}m_*\omega^2 x^2$ we find

$$\omega = \sqrt{\frac{2|t|}{m_*}} \cdot \frac{d|e|B_z}{\hbar}$$

and finally the energy spectrum

$$E = -2|t| + \hbar\omega\left(\nu + \frac{1}{2}\right) = -2|t| + \sqrt{\frac{2|t|}{m_*}} \cdot d|e|B_z\left(\nu + \frac{1}{2}\right) \approx$$
$$\approx -2|t| + \sqrt{2|t|}dB_z(2\nu + 1) \times 0.0256 \text{ meV} \qquad (2.8)$$

where B_z is to be taken in T, t in meV and d in nm. The requirement $E \ll 2|t|$ reads

$$B_z \ll \frac{\sqrt{2|t|}}{d} \cdot \frac{78.1}{2\nu + 1}$$

or introducing a new dimensionless parameter α

$$\alpha \cdot \left(\nu + \frac{1}{2}\right) = \frac{1}{2} \cdot \frac{d|e|B_z}{\sqrt{2|t|m_*}} \cdot \left(\nu + \frac{1}{2}\right) \lesssim 1. \qquad (2.9)$$

---

[6]This is the effective–mass–approximation for the y direction.

The last equation suggests that the qualitative behaviour of the bands (i.e. whether they are flat or parabolic–like) depends only on the single dimensionless parameter $\alpha \cdot \left(\nu + \frac{1}{2}\right)$. This can be verified by rearranging the equation system (2.3) in the following way:

$$|t| \sum_{j=1}^{N} \widehat{H}_{jl}(k_x)a_j = E(k_x)a_l, \text{ where} \qquad (2.10)$$

$$\widehat{H}_{jj} = \alpha^2 \left[j + \frac{k_x}{K}\right]^2, \quad \widehat{H}_{jj\pm 1} = -1.$$

If we investigate only the "first Brillouin zone" for k_x, the term k_x/K ranges from $-\frac{1}{2}$ to $\frac{1}{2}$ and even the whole system of equations depends only on α (t in front of the sum is only a scaling factor for the energy). The bands (indexed by ν) should be almost flat if $\nu < 1/\alpha - \frac{1}{2}$ and almost parabolic if $\nu > 1/\alpha - \frac{1}{2}$.

2.2.3 Numerical Results

Possible Types of the Spectra

In this part we will display the density of states rather than the dispersion relations $E_i(k_x)$ that are the output after solving Eq. 2.3 or 2.10. The relations $E_i(k_x)$ are processed into the density of states by means of Eq. 2.6 or 2.7. For the sake of clarity we also display (see Fig. 2.6) the DOS corresponding to the spectrum shown on Fig. 2.3.

As it follows from Eq. 2.10, the band structure displayed in units $E/2|t|$ depends only on a single parameter α.

Let us consider a sample which is characterized by a field–independent constant $\alpha/B_z \ll 1$ (see the defining Eq. 2.9). Such a sample is suited for Shubnikov–de Haas measurements (in low magnetic fields) since as α remains smaller than 1 even for $B_z \approx 1$ T. A way how to obtain samples with small α/B_z is to decrease the period of the superlattice (d); increasing the coupling constant t leads to a collapse of the simple tight–binding model.

The lowest bands should now be flat and those beginning from index ν_{max} such that $\alpha(\nu_{max} + \frac{1}{2}) \approx 1$ should be parabolic. In order to demonstrate that we chose a sample with $|t| = 0.95$ meV and $d = 15$ nm, i.e. $\alpha/B_z \approx 0.279$ T^{-1} and set $N = 30$. In the Fig. 2.5 we deal with the case $1/\alpha \approx 11$, what
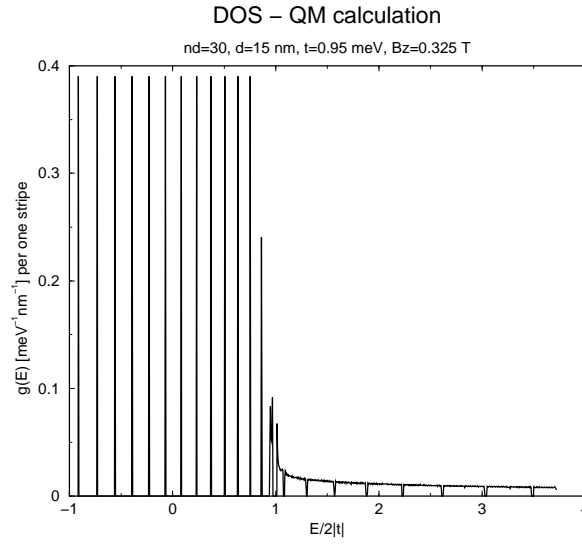
Figure 2.5: Density of states in a weak field ($\alpha \ll 1$).

means $\nu_{max} \approx 11$, i.e. 12 bands. We can distinguish 13 flat bands in the figure.

Increasing the parameter α (by means of increasing the magnetic field) we first get a spectrum like on Fig. 2.6 as we approach $\alpha \approx 1$ where the sharp peaks can still be recognized. At last (for $\alpha > 1$) we make the first Landau band to span up to energies comparable to $2|t|$ (see Fig. 2.7). There is no observable periodic structure for $E < 2|t|$, gaps shift to high energies and become very narrow except for the first one.

Figure 2.6: Density of states for intermediate fields ($\alpha \approx 1$). See the corresponding band structure at Fig. 2.3.

Figure 2.7: Density of states for strong fields.

Relation between the Low–Field Spectra and Zero–Field Spectra

As it was already mentioned in the Semiclassical approach paragraph, the problem described at the very beginning of the paragraph 2.2.1 can be solved a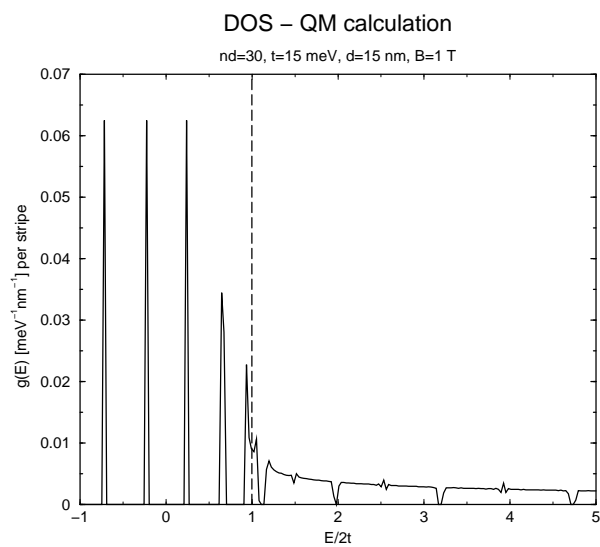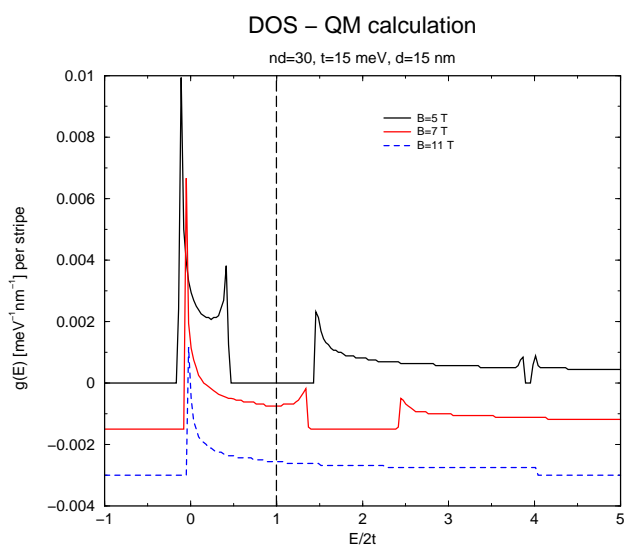nalytically if $\boldsymbol{A} = 0$ (and $N \to \infty$). We start with Eq. 2.1, use the tight binding model and obtain the spectrum

$$E(k_x, k_y) = \frac{\hbar^2}{2m_*}k_x^2 - 2|t_0| \cos k_y d \, . \tag{2.11}$$

The density of states can be calculated analytically out of this spectrum, too (see Appendix A). It exhibits a logaritmical singularity at $E = 2|t|$ and it decays as $1/\sqrt{E}$ for $E \to \infty$, see Fig. 2.8.

This plot seems to be very different from the (numerically calculated) density of states of a system in a weak field (i.e. $\alpha \ll 1$), see for instance Fig. 2.5. However, the spectra at Fig. 2.5 refer to zero temperature. To compute the non–zero spectrum we use the standard relation

$$g(E_F, T) = -\int_{-\infty}^{\infty} \mathrm{d}E \frac{\mathrm{d}f_{FD}(E)}{\mathrm{d}E} g(E) \, ,$$

where $f_{FD}(E)$ denotes the Fermi–Dirac distribution at temperature T and with chemical potential $\mu = E_F$. The effect of this procedure (for $T \approx 1$ K) is shown at Fig. 2.8. The continuity of the DOS behaviour for $B \to 0$ is thus recovered.

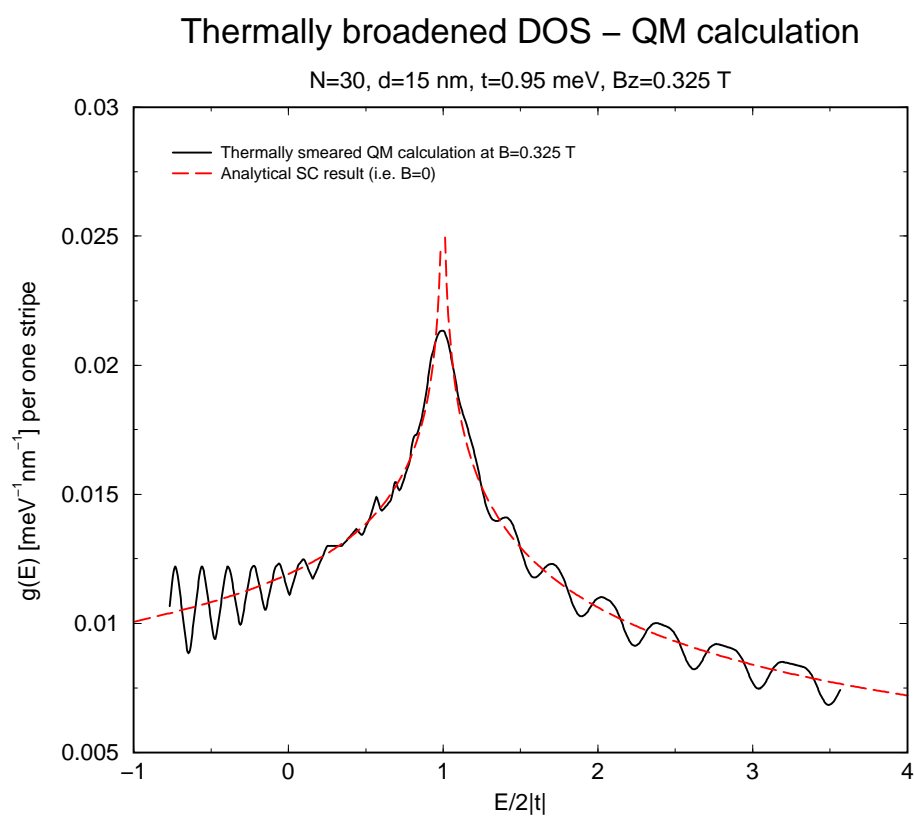Figure 2.8: The density of states for $B = 0$ (dashed) and thermally broadened $(T \approx 1 \text{ K})$ density of states for low field $(\alpha \ll 1$, full line).

Yet we would like to point out another feature of (especially) low–field spectra. According to the discussion following the Eq. 2.10 (and as it was also shown e.g. at Fig. 2.5) the bands are flat and almost equidistant in E for $E < 2|t|$ (the lower is E the better these two properties apply) and the bands are almost parabolic for $E > 2|t|$. It implies that the gaps (between the bands) will be approximatelly periodic in E^2 for $E > 2|t|$ because the gaps can only appear either in the centre or at the edge of the Brillouin zone (see Fig. 2.3).

Followingly if we put the total number of states[7] N under the Fermi level in zero field onto the horizontal axis instead of the Fermi level itself, the ripples (or the gaps) seen on the low–field DOS plots at Figs 2.5,2.8 will be nearly periodic in N both for $E < 2|t|$ and $E > 2|t|$. There will still be some irregularities near to $E \approx 2|t_0|$ though. The reason is that N is an almost linear function of E for E deep under $2|t|$ (as the constant term in DOS is large compared to the linear and next terms) and it is (up to an additional constant) proportional to $\sqrt{E}$ high above $2|t|$ (as DOS is proportional to $1/\sqrt{E}$, see also Fig. 2.9).

We will see later that the gaps play a fundamental role in understanding the magnetoresistance measurements.
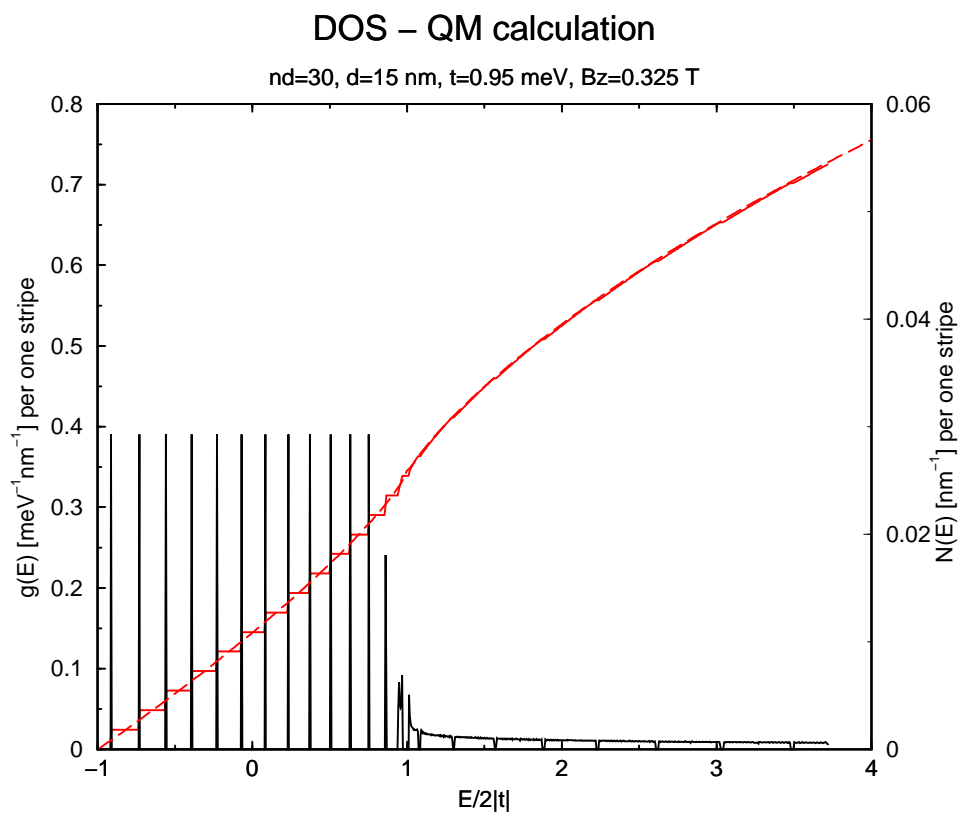
---

[7]See Eq. 2.7.

Figure 2.9: Zero temperature density of states $g(E)$ (line with peaks) and number of states $N(E)$ with energy less than E (dashed: zero field, full line: low field).

2.2.4 Physical Interpretation

Let us make some comments on Fig. 2.8. The singularity in the zero field DOS at $E_F = E = 2|t|$ divides two substantially different regions from each other.

For E_F deep under $2|t|$ and in weak fields the system behaves like an almost free 2D gas in magnetic field. Sharp and nearly equidistant Landau levels (or flat bands) appear, their mutual distance is proportional to B as predicted by Eq. 2.8. This means that if we keep E_F constant (deep under $2|t|$) and change B, the Landau levels are passing through E_F periodically in $1/B$. Although there is not a straightforward relation between DOS and conductivity of the sample, this reminds us of the Shubnikov–de Haas oscillations. We stress that this is the behaviour of a free 2D electron gas, too.

However, the Landau levels remain sharp for the free 2D electron gas even for strong fields. On contrary we can see at Figs. 2.6,2.7 that for sufficiently strong fields the Landau levels broaden even for E deep under $2|t|$.

We now return to the Fig. 2.8. The singularity in the zero field DOS at $E_F = 2|t|$ corresponds to critical semiclassical trajectories as it was already discussed in the paragraph 2.1.2.

In the case of $E_F > 2|t|$ the system approaches the one–dimensional zero magnetic field behaviour. The density of states is (except for the narrow gaps) $\propto 1/\sqrt{E}$, the same as the DOS of a free 1D electron gas. It might be more instructive to see the band structure plot at Fig. 2.4 instead of the DOS: we can see that the spectrum is nearly parabolic (as the one of a free $1D$ electron gas) for $E_F > 2|t|$.

On the other hand, if $E_F > 2|t|$ is not very far from $2|t|$ we will be able to percept the gaps which will be passing through E_F when we change B. Due to this we will observe conductivity oscillations again. The higher E_F will be, the harder will be the perception of gaps and the weaker will be the conductivity oscillations because the gaps get narrower. The free 1D electron gas however has no gaps in DOS.

So as to understand the quantum mechanical results better we will also discuss the mean values of the velocity x component. These are given by

$$\bar{v}_x \equiv \langle \Psi(k_x, n)|\mathbf{v}_x|\Psi(k_x, n)\rangle = \frac{1}{\hbar}\frac{\mathrm{d}E_n}{\mathrm{d}k_x} \ .$$

For the free 2D electron gas it is thus $\bar{v}_x = 0$ while this velocity is non–zero (as the bands are not completely flat) for electrons confined by a superlattice

potential. This can be understood as a non–zero probability of jumping of an electron between two closed trajectories (see Fig. 2.10) which results into a net motion in one direction for electrons with $k_x \approx -\frac{1}{4}K$ and in another direction for those with $k_x \approx \frac{1}{4}K$.

Similarly, compared to the free 1D gas the electrons moving in one direction in a superlattice have a non–zero probability of changing the direction of motion (or jumping between two open trajectories in inverse directions, see also Fig. 2.10). This is a consequence of the fact that there are such values of k_x (near to the end of the Brillouin zone) where $\bar{v}_x = 0$.

These facts are an indication of the breakdown behaviour.

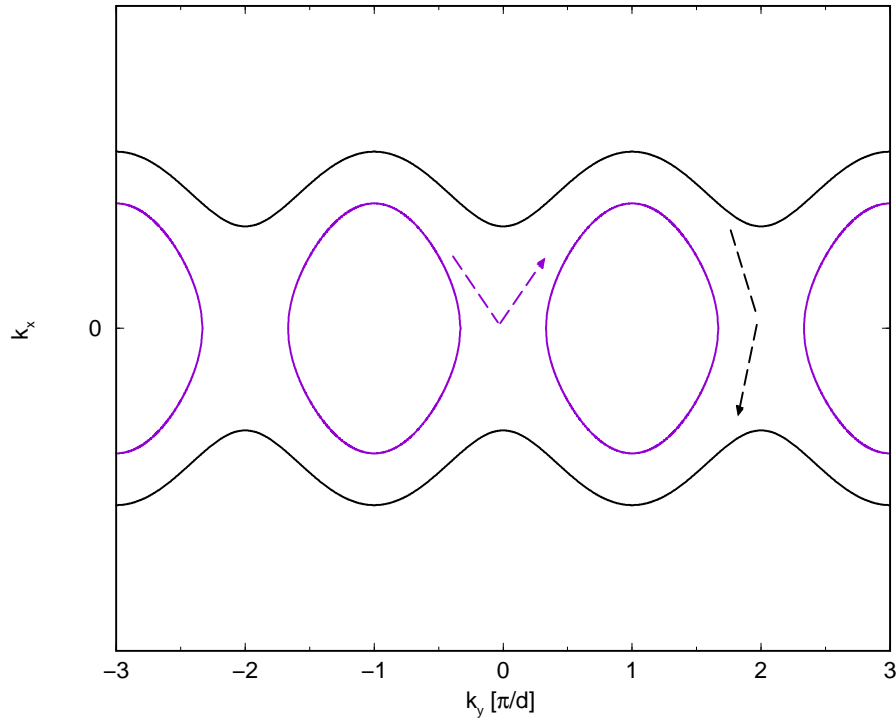## Semiclassical model of the breakdown

Figure 2.10: The semiclassical explanation of the difference between the free electrons and electrons in a superlattice. Unlike the free 1D system the electrons in a superlattice can make some kind of cycles for $E > 2|t|$ or in other words jump between two open orbits.

2.3 Conductivity of a Modulated Two–Dimensional Electron Gas

So far we have shown how to compute the dispersion relations $E_i = E_i(k_x)$ in an approximative way (see Eq. 2.3). We were also able to compute the corresponding eigenfunctions at this point even though we haven't made any use of them yet. The aim of the following section is to establish a general relation between the quantum mechanical solutions of a particular two–dimensional electron gas problem and the components of the electric conductivity tensor.

We are going to use the linear response theory for computing the conductivity tensor components. The starting point will be the formulae for the conductivity tensor diagonal and off–diagonal elements derived by Kubo et al. [10] and Bastin et al. [2], respectively:

$$\sigma_{ii}(E_F) = \pi \hbar e^2 \operatorname{Tr}\left[\boldsymbol{v}_i \delta_\Gamma(E_F - \boldsymbol{H}) \boldsymbol{v}_i \delta_\Gamma(E_F - \boldsymbol{H})\right] \tag{2.12}$$

$$\sigma_{ij}(E) = ei\hbar \int_{-\infty}^{E_F} \mathrm{d}E \ \operatorname{Tr}\left[\boldsymbol{v}_i \frac{\mathrm{d}\boldsymbol{G}^+}{\mathrm{d}E}\boldsymbol{v}_j \delta_\Gamma(E - \boldsymbol{H}) - \boldsymbol{v}_i \delta_\Gamma(E - \boldsymbol{H})\boldsymbol{v}_j \frac{\mathrm{d}\boldsymbol{G}^-}{\mathrm{d}E}\right]. \tag{2.13}$$

The indices i and j stand for x or y, $\boldsymbol{v}_i$ denotes the velocity component operator. We employ the common definition of Green functions which allows us to express delta functions in terms of $G^\pm$:

$$\boldsymbol{G}^\pm(E) = \frac{1}{E - \boldsymbol{H} \pm i\Gamma}\,, \qquad \delta_\Gamma(E - \boldsymbol{H}) = -\frac{1}{2\pi i}(G^+ - G^-)\,.$$

We stress that the original formulae (2.12,2.13) are derived with $\Gamma \to 0+$. However, in this case the conductivities (e.g. for a free electron gas) would be infinite as no scattering mechanism was considered. The effect of elastic scattering on randomly located impurities can be modelled by inserting the complex self–energy term into the Green function (i.e. replacing $[E - \boldsymbol{H}]^{-1}$ by $[E - \boldsymbol{H} - \Sigma(E)]^{-1}$), [9]. If the self–energy has a non–zero imaginary part, the conductivities remain finite. As a model we will further put $\Sigma(E) = i\Gamma$, $\Gamma > 0$, we will keep Γ as a parameter and we are going to examine the $\Gamma \to 0$ asymptotic behaviour. A more detailed treatment of the self–energy method (based on second order Born approximation calculations) is discussed in [9].

The Equations 2.12, 2.13 are a prescription for computing the conductivity tensor components at zero temperature, the Fermi level being E_F. To get their non–zero temperature values we use

$$\sigma_{ij}(T) = -\int_{-\infty}^{\infty} \mathrm{d}E \frac{\mathrm{d}f_{FD}(E)}{\mathrm{d}E} \sigma_{ij}(E) \,, \qquad (2.14)$$

where $f_{FD}(E)$ is the equilibrium Fermi–Dirac distribution normed (by means of E_F) to the particular number (areal concentration) of particles N in system

$$f_{FD}(E) = \frac{1}{\exp(\frac{E-E_F}{kT}) + 1}, \qquad N = \int_{-\infty}^{\infty} \mathrm{d}E g(E) f_{FD}(E) \,,$$

$g(E)$ stands for DOS of the particular electron system.

Let us make a brief comment on the derivation of Equations 2.12, 2.13. These relations can be obtained by integrating the Liouville equation ($\boldsymbol{f}$ is the density matrix operator)

$$\frac{\mathrm{d}\boldsymbol{f}}{\mathrm{d}t} + \frac{1}{i\hbar} \left[\boldsymbol{f}, \boldsymbol{H} + \boldsymbol{H}' \right] = 0$$

and taking into account only the terms linear in the perturbation Hamiltonian $\boldsymbol{H}'$. In our case the perturbation is a homogeneous electric field $\boldsymbol{E}$ and we calculate the current response $\boldsymbol{j}$, i.e. $\mathrm{Tr}(e\boldsymbol{v}\boldsymbol{f})$. Finally, we determine σ_{ij} using the relation $j_i = \sum_j \sigma_{ij} E_j$. This procedure is explained in [9] in a nice and understandable way.

The form of Equation 2.13 is inconvenient from the computational point of view because it forces us to integrate over energies even at zero temperature. A way how to partially avoid this was suggested by Středa in [15]

$$\sigma_{ij}(E) = \sigma_{ij}^I(E) + \sigma_{ij}^{II}(E)$$
$$\sigma_{ij}^I(E) = \mathrm{Tr}\left[\boldsymbol{v}_i \boldsymbol{G}^+(E) \boldsymbol{v}_j \delta_\Gamma(E-\boldsymbol{H}) - \boldsymbol{v}_i \delta_\Gamma(E-\boldsymbol{H}) \boldsymbol{v}_j \boldsymbol{G}^-(E) \right] \quad (2.15)$$
$$\sigma_{xy}^{II}(E) = -\sigma_{yx}^{II}(E) = e\frac{\partial N(E)}{\partial B} \,.$$

The integration over energies remained in $N(E)$ (the total number of particles with energies less than E)

$$N(E) = \int_{-\infty}^{E} \mathrm{d}E g(E) = \int_{-\infty}^{E} \mathrm{d}E \, \mathrm{Tr}\, \delta(E-\boldsymbol{H}).$$

This is however a quantity much simpler to compute numerically.

Before we proceed in applying Equations 2.12,2.15 to our particular system we would like to point out one general feature of these equations in two–dimensional systems. If the Fermi level lies in a gap (i.e. $g(E_F) = 0$), all σ_{xx}, σ_{yy} and σ_{xy}^I vanish whereas the second term of σ_{xy} can be non–zero. If the gap is situated between the l-th and $(l + 1)$-st Landau bands the value of this term will be le^2/h because the areal concentration of states per one Landau band is eB/h (see Appendix B). Thus, σ_{xy} will be constant throughout the gap and equal to an integer multiple of e^2/h which is a quantum-Hall-phenomenon-like behaviour.

2.3.1 Modulated Two–Dimensional Electron Gas

We turn now to the system described by the Hamiltonian (2.1), see also Fig. 2.1. First of all this means the velocity component operator $\boldsymbol{v}_i$ has the form

$$
\begin{aligned}
\boldsymbol{v}_x &= \frac{1}{i\hbar}[\boldsymbol{x}, \boldsymbol{H}] = \frac{1}{m}(\boldsymbol{p}_x - eB\boldsymbol{y}) \\
\boldsymbol{v}_y &= \frac{1}{i\hbar}[\boldsymbol{y}, \boldsymbol{H}] = \frac{1}{m}\boldsymbol{p}_y \,.
\end{aligned}
\tag{2.16}
$$

Further (see paragraph 2.2.1) we recall that the (orthonormalized) approximate solutions to the Schrödinger equation are

$$
\boldsymbol{H}|\Psi\rangle = E(k_x, n)|\Psi\rangle, \qquad |\Psi\rangle = |k_x\rangle \sum_{j=1}^{N} a_j(k_x, n)|j\rangle \stackrel{\text{def}}{=} |k_x\rangle|\psi\rangle \,,
$$

where the ket $|j\rangle$ denotes the lowest eigenstate in the j-th well of the superlattice potential $V(y)$ and it holds within our approximation $\langle j|k\rangle = \delta_{jk}$. The eigenstates take the following form in coordinate representation (see also paragraph 2.2.1)

$$
\Psi(x, y) = \frac{1}{\sqrt{2\pi}} e^{-ik_x x} \sum_{j=1}^{N} a_j(k_x, n) \varphi(y - jd) \,.
$$

As soon as we determine the eigenstates $\Psi(x, y)$ we can compute the traces in Eqs. 2.12 and 2.15.

We have not obtained any reliable results so far because of problems on the numerical level. The expected form of results is however discussed in subsection 2.5.3.

2.4 The Way from Theory to Experiment

2.4.1 The Experimental Setup

The samples were fabricated and measured by R. A. Deutschmann at the Walter Schottky Institute in München. The geometry of the samples measured is shown at Fig. 2.11 and can be obtained using the cleaved edge overgrowth method [4],[5]. The basis of the sample is a 3D GaAs/GaAlAs superlattice (i.e. alternating layers of the two materials) with the period of 15 nm and number of periods 100. The first and the last layer is contacted (source and drain): first there's an undoped GaAs layer (100 nm) and then 1 μm of n+ GaAs. This structure is cleaved in situ perpendicular to the layers and a n+ GaAs gate (with 15 nm undoped GaAs spacer) is grown on the fresh surface.

Figure 2.11: The sample. Reprinted with kind permission of R. A. Deutschmann.

By applying positive voltage to the gate U_g electrons are drawn from the volume of the superlattice to a thin layer at the gate spacer. Thus a 2D electron gas is created which is subject to the superlattice potential. The concentration of electrons in the 2D gas (or consequently chemical potential) is gate–voltage–dependent. If we apply magnetic field perpendicular to the

cleavage plane we arrive at the situation with the geometry shown at Fig. 2.1.

The quantity mesured on this sample is the resistance depending on magnetic field and gate voltage. There are separated voltage and current contacts on both source and drain. However, this setup has to be treated just as a two–point measurement from the point of view of the 2D system (see Fig. 2.12). The reason why this is an important issue is that there are two mechanisms of electron transport in the y direction: the bulk states conductivity and the edge states conductivity[8]. Using the two–point measurement geometry (Fig. 2.12a) we measure a result of a mixture of the two phenomena (see below) while in the four–point scheme (Fig. 2.12b) both longitudinal and transversal voltages can be measured allowing thus to separate the two conductivity contributions. This topic is naturally discussed in some papers concerning the quantum Hall effect.
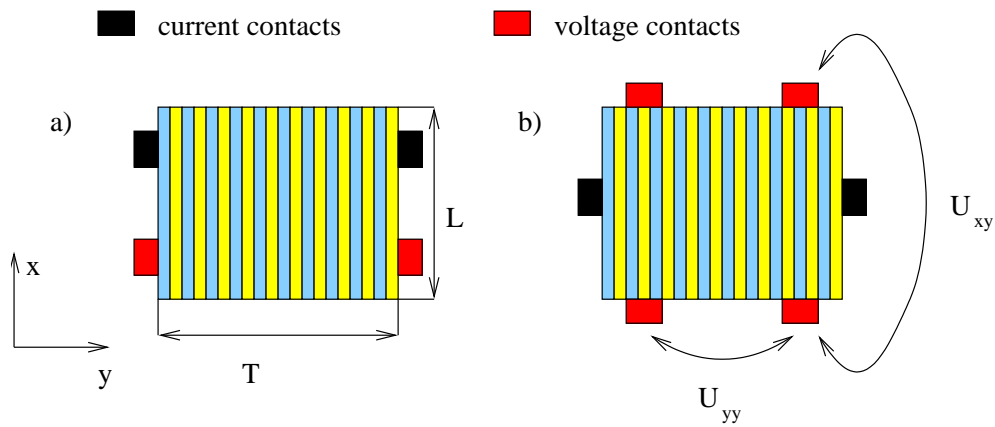

Figure 2.12: 2D superlattices: (a) two–point measurement, (b) four–point measurement.

Four–Point Measurement

Let us now sketch how to use the advantage of a four–point measurement. Due to the presence of the magnetic field the 2D gas will be strongly anisotropic

---

[8]We stress that this is only one of theories explaining the quantum Hall effect which is still not proven to be the only correct one.

and the total current passing through the 2D superlattice (in the y direction) will be given by the conductivity σ or resistivity ϱ *tensors*

$$j_y = \sigma_{xy} U_{xy} + \sigma_{yy} U_{yy}, \quad \text{or} \qquad\qquad (2.17)$$

$$U_{xy} = \varrho_{xy} j_y \quad \text{and} \quad U_{yy} = \varrho_{yy} j_y \,,$$

because j_x (transversal density of current) vanishes. There are some symmetries of σ: first $\sigma_{xy}(B) = \sigma_{yx}(-B)$ (Onsager relation [1]) combined with $\sigma_{xy}(B) = -\sigma_{xy}(-B)$ and $\sigma_{yx}(B) = -\sigma_{yx}(-B)$ (Hall current changes direction when $\boldsymbol{B} \to -\boldsymbol{B}$) yields $\sigma_{xy}(B) = -\sigma_{yx}(B)$.

The tensors σ and ϱ are inverse to each other which gives (with respect to the symmetries of σ)

$$\varrho_{yx} = -\varrho_{xy} = -\frac{\sigma_{yx}}{\sigma_{xx}\sigma_{yy} + \sigma_{yx}^2}, \quad \varrho_{xx} = \frac{\sigma_{yy}}{\sigma_{xx}\sigma_{yy} + \sigma_{yx}^2}, \quad \varrho_{yy} = \frac{\sigma_{xx}}{\sigma_{xx}\sigma_{yy} + \sigma_{yx}^2} \,.$$
$$(2.18)$$

The voltages U_{xy} and U_{yy} can be measured in the four–point scheme and thus σ_{xy} and σ_{yy} can be calculated as a function of $|\boldsymbol{B}|$.

Two–Point Measurement

We will now sketch the way how to estimate the experimentally measured resistance assuming that we have done only the DOS calculation.

Let us think of the sample as of a conductive slab (see Fig. 2.12,a) characterized by two conductivity components $\sigma = \sigma_{xx} = \sigma_{yy}$ and $\sigma_H = \sigma_{xy}$; the thickness T (in the y direction) of the slab is substantially less than its length L (in the x direction). A two-terminal resistance R can be found out from the voltage difference U measured across the source and drain contacts and is given by $R = U/I$, provided the current passing through the sample being I.

A two-terminal resistance of rectangular slabs subject to perpendicular magnetic fields was studied both theoretically and experimentally e.g. by Rikken et al. [12], but their results hardly apply in our case ($T \ll L$), which is far away from the standard Hall bar geometry.

For small Hall angles $\varphi_H \overset{\text{def}}{=} \arctan(\sigma_H/\sigma)$, i.e if $\varphi_H \ll \arctan(T/L)$, our sample reminds the Corbino disc (see Fig. 2.13) in some aspects. Far away from the edges, the electric field is perpendicular to the source and drain contacts and $E = U/T$. The current flow deviates from this direction by the
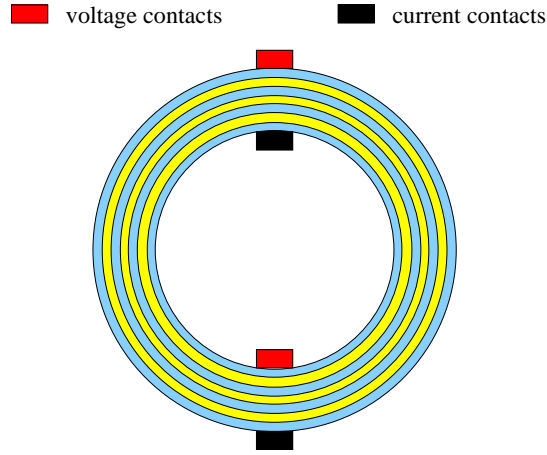
Figure 2.13: Corbino disc geometry.

Hall angle and only a very small part of electrons near the edges does not obey the rule. In this case

$$R \approx \frac{1}{\sigma} \frac{T}{L}, \tag{2.19}$$

similarly as for the Corbino disc. In the quantum Hall regime $\sigma \to 0$ and R should diverge for a true Corbino disc.

In our sample, the limit $\sigma \to 0$ means that $\varphi_H \to \pi/2$ and consequently φ_H becomes larger than $\arctan(T/L)$. Then, in spite of its thickness to length ratio, our sample behaves like a standard Hall bar for which the two–terminal resistance is known [12] to be very close to the quantized Hall plateau resistance, $R \approx h/(e^2 \cdot i)$, where i is a positive integer number. Thus, in our case R does not diverge as the singularity is cut off by the resistance of the corresponding Hall plateau.

Both σ and σ_H are complicated functions of magnetic field and concentration of carriers. If the Hall angle never becomes small for a given concentration (but deviates from $\pi/2$ substantially), the Eq. 2.19 does not apply for any field. It is known [12] that in this case R is given by a combination of ρ and ρ_H which are related to σ and σ_H by

$$\rho \approx \sigma/\sigma_H^2, \qquad \rho_H \approx 1/\sigma_H \ . \tag{2.20}$$

This ϱ's to σ's correspondence is given by relation 2.18 provided that $\sigma \ll \sigma_H$.

The weak point of this approach is that the slab (2DEG) is strongly anisotropic ($\sigma_{xx} \neq \sigma_{yy}$). Even though we can estimate that $\sigma_{yy} \ll \sigma_{xx}$ we are not able to predict whether $\sigma_{xx}\sigma_{yy}$ is smaller or greater σ_{xy}^2 in a Landau level. In the latter case the Eq. 2.19 describing the measured resistance is substituted by relations (2.20).

A consequence is that knowing DOS only we have no indication on the value of σ (for E_F in a Landau level) compared to the known σ_H in the gaps — even for small Hall angles. It is thus impossible to predict whether the Hall plateaus of the measured resistance will be maxima or minima.

Concluded, we can only say that in the two–point scheme there should appear the Hall plateaus if the Fermi level lies in a gap. We will make several comments on the general relation between DOS and σ, σ_H in the next paragraph.

2.4.2 Relation between Conductivity and Density of States: A Simple Model

It is a rather complex problem to find a good approximation which would lead us from the calculated spectrum and eigenstates up to the conductivity. Later we will show the results of Kubo formula (linear response theory) which is however not very easy to follow (see section 2.3). We will discuss the possible shape of the relation now in a very rough way which will give us better insight into the matter. We focus at the two–point scheme now.

One of the contemporary theories attempting to explain the Quantum Hall phenomenon concerns the *edge states* [3]. We will sketch the idea briefly: Landau levels in a finite 2D free electron gas rise in the vicinity of edges — from the semiclassical point of view the electrons move on circular orbits no longer and take cycloidal trajectories. The energy of these states is higher than the one of the corresponding bulk (circular orbit) states and (assuming that the 2DEG is confined to an infinitely deep well) it grows to infinity as these orbits approach the edge. Thus if the Fermi level lies in the gap between i-th and $(i+1)$-th bulk Landau level it crosses the i lower Landau levels in the edge region. These intersections represent the *edge states*. It can be derived [3] that each edge state contributes to the conductivity by e^2/h. The total conductivity in this case is thus ie^2/h and it *doesn't depend on where in the gap the Fermi level is*.

Further on we will thus assume that there are two parallel channels of

electron transport in the sample — the bulk states conductivity and the edge states conductivity. The relation (2.17) gives us a hint how the two channels could be related to the conductivity tensor: the diagonal components (σ_{xx}, σ_{yy}) describe the bulk conductivity and the off–diagonal component (σ_{xy}) reflects the edge–states conductivity[9]. We also recall that the transport concerns electrons near to the Fermi level only. The appropriate quantity will thus be the density of states (DOS) at the Fermi level, for non–zero temperatures we will use the standard relation (2.14).

We will estimate the conductivity of the two channels now. The simplest model is that the bulk conductivity grows with increasing density of states. In particular, $\sigma_{ii} = 0$ if Fermi level lies in the gap and is non–zero in a Landau level.

The edge states conductivity is ie^2/h if the Fermi level lies in a gap. We have however no estimate for it in the other case. Note that there's also another cotribution to σ_H originating from the classical Hall phenomenon.

Concluded, the simplest DOS–based model of the magnetoresistance is that we measure the resistance $(1/i) \cdot h/e^2$ in the gap and $c \cdot 1/g(E_F)$ in a Landau level (if the edge states conductivity is negligible to the bulk states one). The proportionality constant c can be however a function of E_F (and we might only hope that it is varying slowly). We stress once again that we cannot predict whether the Hall plateaus lie below or over the typical bulk states resistance.

2.4.3 The Relation Between Gate Voltage and Fermi Energy

We divide this problem into two steps. The first one is the relation between the gate voltage U_g and concentration of electrons N in the 2D gas. We assume that this relation is a proportionality. This means that the gate structure works as a capacitor which seems to be a plausible model.

The second step is to find the relation between Fermi energy and N. The usual relation is

$$N(E_F) = \int_{-\infty}^{E_F} g(E)\,\mathrm{d}E.$$

Here, $g(E)$ must be computed from the zero–temperature DOS (as shown e.g. on Fig. 2.6) to which the thermal broadening relation is applied (2.14).

---

[9]This is a naive model and it will be replaced by a better one in the subsection 2.5.3.

Thus, for low fields and *non–zero temperatures* the relation $N = N(E_f)$ can be also roughly approximated by the zero field relation at zero temperatures (5.1), see Fig. 2.8 and the corresponding paragraph.

Overlaying the experimental and theoretical 2D plots on each other we can now determine the proportionality constant between U_g and N. The aim is that the gaps of DOS match the straight resistance minima lines (for weak fields and high gate voltages). Typical value of this constant is 6×10^{11} cm^{-2}V^{-1}.

Agreement between the theoretical and experimental graphs gives us thus a feedback: the assumption $N \propto U_g$ is now justified.

2.4.4 Coupling Constant

We could see that the parameter t which describes the strength of coupling between two neighbouring wells plays an important role in the theoretical calculations. Up to now, our concept that we do not know anything about the superlattice potential $V(y)$ except for its period d and the coupling constant t. However, in our specific case we can consider $V(y)$ to be rectangular and we also know the depth of the wells which equals the GaAs/GaAlAs band offset.

Exploiting thus our knowledge about the sample structure we can employ the Kronig–Penney model and determine the spectrum of the system in zero magnetic field. The result is[10] $E(k_x, k_y) \approx \hbar^2 k_x^2 / 2m_* - \Delta/2 \cdot \cos k_y d$ where the width of the first miniband is $\Delta \approx 3.8$ meV (see [5]). Comparing this to the tight–binding approximation zero field spectrum (2.11) we obtain $t \approx 0.95$ meV.

Let us also make a short comment on the assumption that only the ground state in each well is occupied which was a basis for the ansatz (2.2). It was computed by [5] within the Kronig–Penney model that the second miniband lies 60 meV above the first one which is sufficiently more than the Fermi energies at relevant carriers concentrations (e.g. for $N = 5.9 \times 10^{11}$ cm^{-2} it is $E_F \approx 8.9$ meV).

---

[10]The band part of this spectrum has not an exact cosine form.

2.5 Experimental Results and Comparison to the Theory

All the experimental results were obtained by R. A. Deutschmann at the Walter Schottky Institute in München and are reprinted with his kind permission.

2.5.1 Experimental Results

As it was mentioned above, both magnetic field and gate voltage can be changed during the experiment. The measured quantity is the voltage drop on the sample at a given current ($I = 10$ nA for the data displayed). The current voltage characteristics was found to be linear for low currents and thus the measurements were presented as sample resistance measurements for different gate voltages and magnetic field strengths. The measurement outcome can be displayed as a 2D plot (see Fig. 2.14). However, the measured resistance ranges within more orders of magnitude while important structures are in some regions quite weak. We used two methods of displaying the data so as to emphasize these features. We employed logaritmical scale for resistance and subtracted linear background (fitted by the least square method) at Fig. 2.14 (top) and plotted the resistance R transformed using formula $R \mapsto (\partial^2 R/\partial U_g^2)/|\partial R/\partial U_g|$ at Fig. 2.14 (bottom). The latter method shows the fine structure better but it rather shows the steepness of the extrema than the value of the plotted function (i.e. does not distinguish deep and shallow extremes). The former method gives a better global overview.
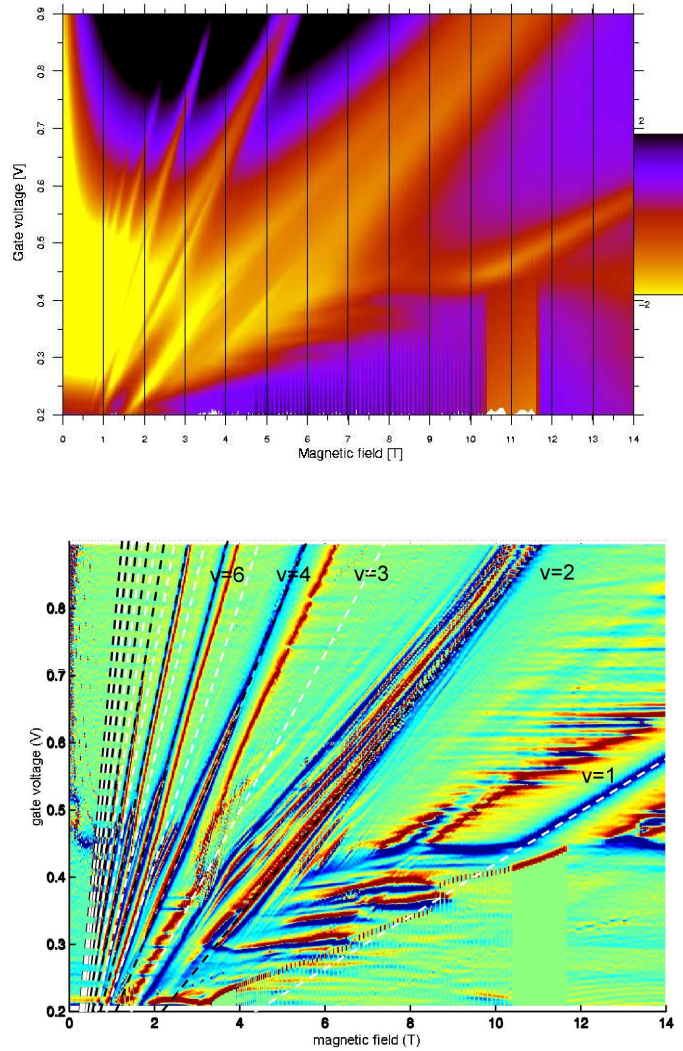
Figure 2.14: Experimental data: field– and gate–voltage–dependent resistance (in arbitrary units) of the sample. The same data processed by two different methods: logarithmical scale (top) and derivatives method (bottom). Reprinted with kind permission of Rainer Deutschmann.

2.5.2 DOS Calculations

We have already shown how to compute the density of states as a function of energy E for different magnetic field strengths. By merging these plots (as e.g. the one at Fig. 2.5) into one 2D plot and transforming E (Fermi energy) into N on the vertical axis, the zero field number of states under E (using Eq. 5.1) we obtain Fig. 2.15 (left plot). The dark regions correspond to the Landau bands, the light regions are the gaps.

As it was already mentioned before we further assume that N is proportional to the gate voltage U_g. We determine the proportionality constant so that the theoretical plot would match the experimental plots (at Fig. 2.14), namely that the lines corresponding to gaps and the lines of resistance minima have the same position. In our case we found out its value to be 7.0×10^{-11} cm^{-2}V^{-1} and obtained the right plot on Fig. 2.15.

We can see that the structures of the theoretical and experimental plots are in a good agreement except for the resistance minimum starting at $B \approx$ 8 T and $U_g \approx 0.4$ V which has no counterpart in the theoretical plot. It shows that our model is not valid in this region. This can be due to the fact that the ansatz (2.2) has no justification if the electron cyclotron radius becomes very small compared to the superlattice period d and the state is thus strongly localized in a single well (or in other words the tunnelling between two adjacent superlattice wells is negligible due to the magnetic field).

Despite this mismatch we can see that the used model gives a good description of the system in all other regions.
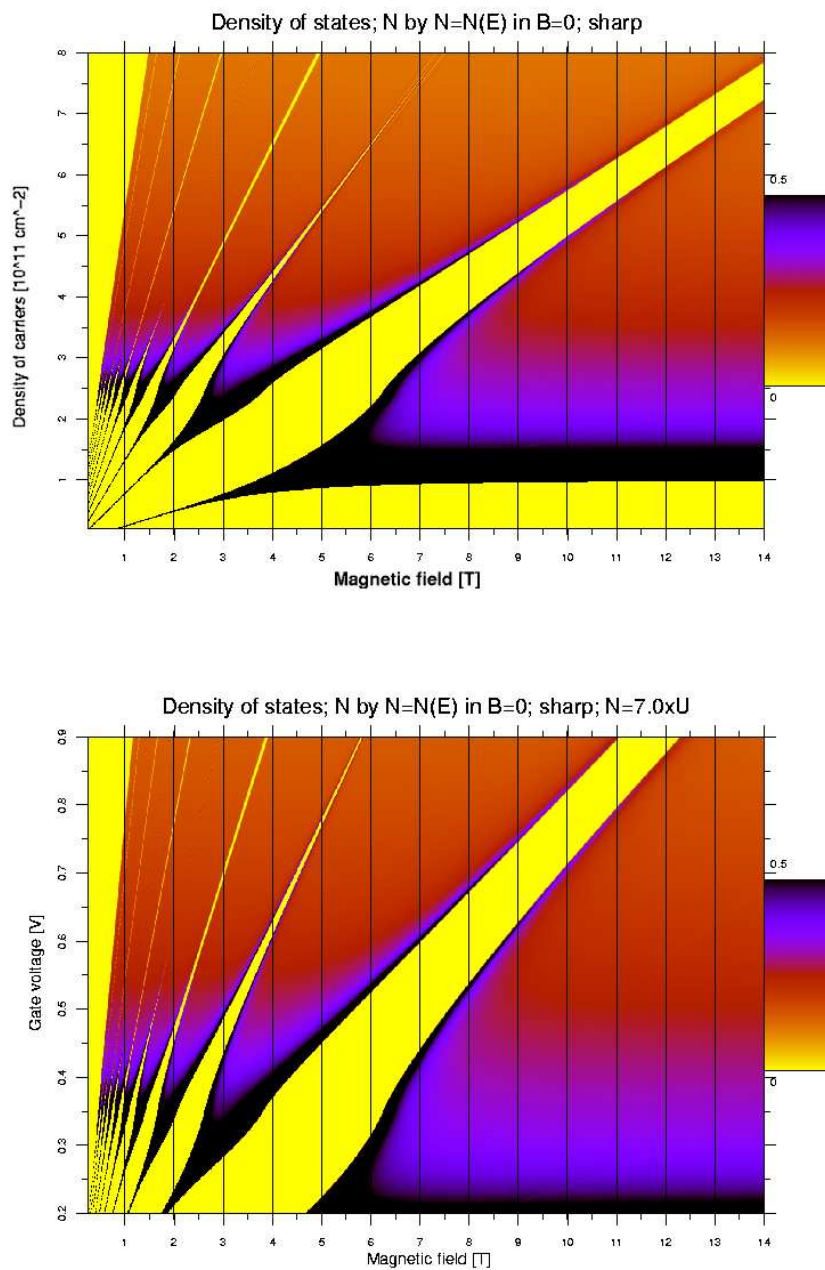
Figure 2.15: DOS calculation: B is on the horizontal axis on both plots. On the vertical axis there is the zero field number of states (left) and the gate voltage (right).

Another type of insight give the sections of the 2D plot, i.e. graphs of field–dependent resistance at (different) constant gate voltages U_g. Very clear pictures can be obtained by plotting more lines (i.e. at different U_g) into one graph with B/U_g instead of just B on the horizontal axis, see Fig. 2.16. So as to be able to compare these plots with the theoretical results we again assumed that the gate voltage is proportional to the total number of carriers (see above). Note that under this assumption the horizontal axis is proportional to the reciprocal value of filling factor (i.e. one over number of Landau levels occupied).

However, the match of theory and measured data is only very rough at the level of DOS. It has already been suggested above that we cannot predict whether the resistivity will have a maximum or minimum for E_F lying in gap from the semiclassical point of view. On the other hand we can see that the resistivities (for various values of N) approach the same value 12.9 kΩ around $B/N \approx 2$. This is the resistivity of the first Hall plateau ($\frac{1}{2}h/e^2$, one half for the spin) and that can be predicted without the Kubo theory.
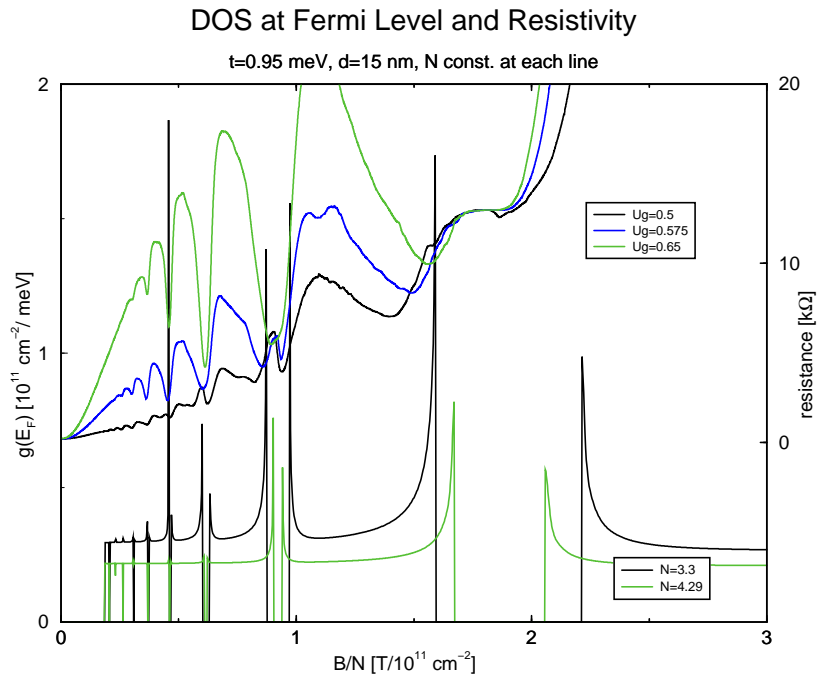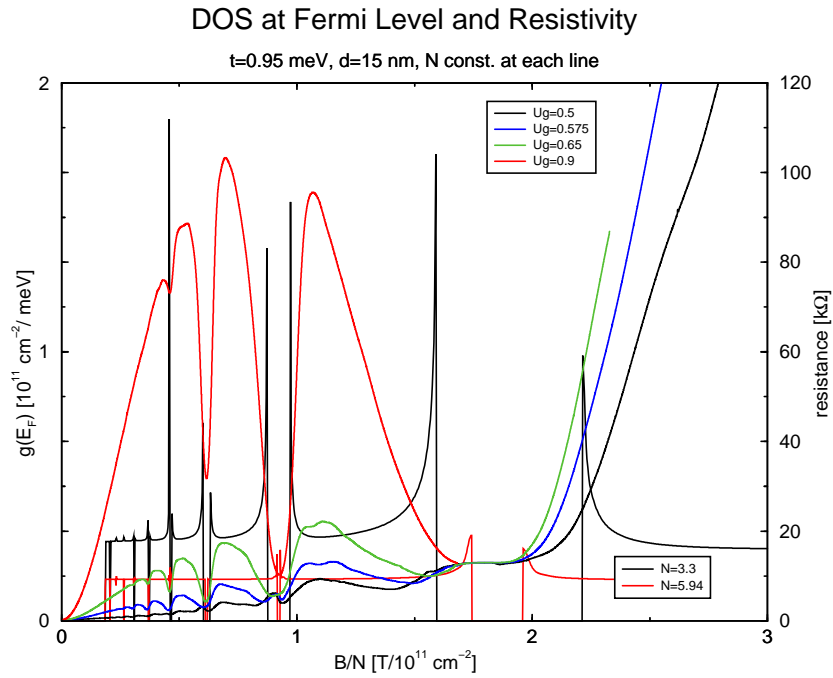
Figure 2.16: Experimental data along with calculation results: field–dependent resistance of the sample for different gate voltages. Smooth curves are the experimental data (U_g in volts), curves with singularities are the calculations of DOS (N in 10^{11} cm^{-2}). Experimental and DOS curves of the same colour correspond to the same gate voltage ($U_g = 6.6 \cdot N$). Reprinted with kind permission of Rainer Deutschmann.

2.5.3 Kubo Formula Calculations

We have already presented a way how to compute the conductivity components in the subsection 2.3.1. Subsequently we use the formulae (2.18) to transform them into the resistivity components. Due to numerical problems which occur when evaluating the traces (Eq. 2.15) we have not obtained any final results yet but we believe that the main features of the B–dependent resistivity to be measured are included in our present R_{yy} plot[11] (see Fig. 2.17).

First of all we found out that R_{yy} vanishes in the gaps. If the Fermi level lies in a gap then the only non–zero component of resistivity will be R_{xy} which is then equal to the quantized Hall resistance $h/(2e^2 n)$, $n = 1, 2, \ldots$ We can also see on the plot (2.17) that the lower is the magnetic field the thinner are the gaps and the less pronounced are thus the minima of R_{yy} at the positions of gaps. Another important point is that the gaps get thinner also when concentration of electrons (N) increases and thus at higher concentrations less periods of oscillations can be distinguished (as it can also be seen in the experimental data). It can also be recognized that the envelope function of the plotted R_{yy} is similar as the one of the experimental magnetoresistance: right from the first Hall plateau ($R \approx 12.9$ kΩ in the figure) it grows rapidly and approaches zero between this plateau and zero field with a maximum approximatelly in the centre.

As it was already mentioned before we had to take into account scattering of electrons on impurities in order to avoid infinite conductivities. This effect was modelled by including the imaginary part Γ of the self–energy into the Green function which was kept further on as an unspecified parameter. We found out that variation of its value causes only that R_{yy} is scaled by $1/\Gamma$. This gives us some justification to consider the plot (2.17) as relevant.

We empasize however that the self–energy (and thus also Γ) *is* E_F–dependent (or concentration–dependent), see [16] or [11].

Let us now make a short comment to the relation between the resistance components and the experimental data. We recall the relations (2.17):

$$U_{xy} = R_{xy} I_y \quad \text{and} \quad U_{yy} = R_{yy} I_y \,.$$

As we use the two–point measurement scheme (see Fig. 2.12a) we cannot measure U_{xy} and U_{yy} separately; what we measure is a mixture (a weighted

---

[11]We leave the current densities j and switch to the current I. Subsequently the resistivity ϱ will be replaced by resistance R.

mean) of these two values. However if the Fermi level lies in a gap, the R_{yy} component vanishes and we thus measure U_{xy} only.

In the other cases (DOS non–zero) we expect that R_{xy} does not deviate dramatically from the smooth transition between the two adjacent Hall plateaus values (see [13]) and thus the total voltage measured will be influenced by R_{yy}. This seems to be the case of the high concentrations (see e.g. the plot for $N = 5.94 \times 10^{11}$ cm^{-2} on the Fig. 2.16).

Let us now summarize the arguments illustrating the agreement between the experiment (Fig. 2.16) and theory (Fig. 2.17).

1. The *critical points* (maxima or minima for different concetrations) which correspond to the Fermi level positioned in a gap match perfectly.

2. The Hall plateaus in gaps are reproduced by the theory (note that the plateaus have the resistances $R_i = h/(2e^2 i)$, $i = 1, 2, \ldots$, the factor of two corresponds to spin).

3. The resistance rises rapidly right from the first Hall plateau ($B/N > 2 \times 10^{-11}$ Tcm^2).

4. Envelope functions of the resistances left from the first Hall plateau have the same shape.

5. The lower is the concentration the more pronounced are the resistance critical points (minima).
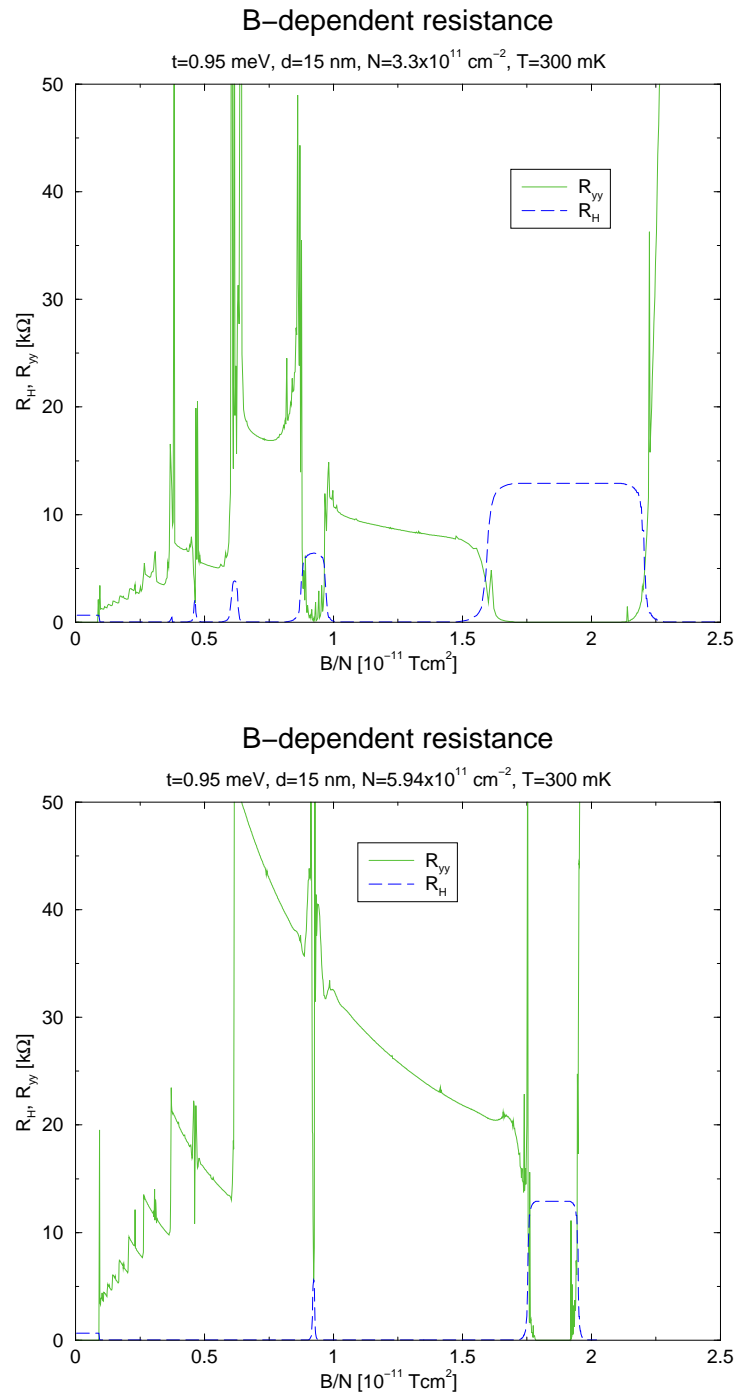
Figure 2.17: Kubo formula calculations of R_{yy} for two different concentrations of carriers. Dashed lines show the positions (and resistances) of the Hall plateaus.

Chapter 3

Three–Dimensional Superlattices

3.1   Introduction

3.1.1   Description of the System

The superlattices investigated in this part are considered to be described by one–dimensional potential $V = V(z)$ having a period of d_z, see Fig. 3.1. The
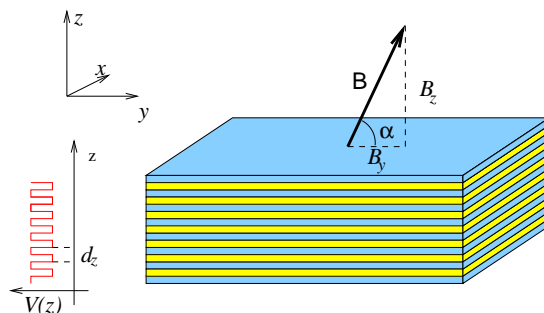
Figure 3.1: A three dimensional superlattice.

exact shape of the potential is not specified, we only assume that there is one well in each period and describe the potential by means of the coupling constant assigned to ground states in two neighbouring wells (see below).

The movement of electron in planes perpendicular to z axis is free.

Such a structure can be fabricated using epitaxial methods. Magneto-transport measurements on InGaAs/InP structures were performed for instance by Jaschinski [8].

Unlike the case of the two–dimensional systems, magnetic field will now be applied in an arbitrary direction. By *perpendicular* field we mean field parallel to the z axis, otherwise we will speak of *tilted* field.

3.1.2 Semiclassical Approach

The concept of the semiclassical (SC) description of 3D systems is an extension of the SC theory mentioned in the subsection 2.1.2. The tight–binding zero–field spectrum of the 3D system is

$$E(k_x, k_y, k_z) = \frac{\hbar^2}{2m_*}k_x^2 + \frac{\hbar^2}{2m_*}k_y^2 - 2|t_0|\cos k_z d_z . \qquad (3.1)$$

The Fermi surfaces $E_F = E(k_x, k_y, k_z)$ take three topologically different forms which all posses rotational symmetry as the system is isotropic in the x, y plane. These surfaces can be obtained by rotating the curves 0, 1 and 2 of Fig. 2.2 around the $k_x = 0$ axis. The forms can thus be (a series of) deformed (rotational) ellipsoid for $E_F < 2|t|$ or a corrugated cylinder for $E_F > 2|t|$; the transition Fermi surface between these two regions is a series of just touching spindle–like bodies.

In order to determine the semiclassical trajectories of an electron if the system is subject to magnetic field $\boldsymbol{B}$ we have to construct a cross section of the Fermi surface by a plane perpendicular to the magnetic field direction. By rotating these curves by 90 degrees around $\boldsymbol{B}$ and scaling them by $\hbar/(|e||\boldsymbol{B}|)$ we get the real space trajectories. Note that there is a whole class of such trajectories for each direction of $\boldsymbol{B}$ (which can be obtained by shifting the section plane along $\boldsymbol{B}$).

Compared to the 2D system there is now a larger variety of trajectory shapes because they depend both on Fermi level value and on the field direction. Nevertheless, all trajectories are closed for $E_F < 2|t|$ even in the 3D case. For $E_F > 2|t|$ the trajectory can be either open or closed, depending on the field direction.

There is the quantization condition again which requires the *closed* trajectories to enclose area $A(E_F)$ equal to an integer multiple of magnetic flux

quanta $|e||\boldsymbol{B}|/h$ (in the k–space)

$$A(E_F) = n \cdot \frac{|e||\boldsymbol{B}|}{h}, \quad n = 1, 2, \ldots . \tag{3.2}$$

Shubnikov–de Haas oscillations

Let the Fermi level E_F and the magnetic field direction be fixed and consider the class of the closed trajectories indexed by a parameter ξ which corresponds to the section plane shift in the direction of $\boldsymbol{B}$. Due to the quantization condition (3.2) only some of the trajectories are permitted. If we vary the field strength $|\boldsymbol{B}|$, one or more of the permitted trajectories may fulfill $\partial A(E_F)/\partial \xi = 0$. It means that there are many other trajectories near to this one which enclose area near to $A(E_F)$. The SC theory claims that this should correspond to singularity of the density of states.

Thus the SC theory suggests to find *extremal cross–sections* A_{max}, A_{min} of a Fermi surface (for a given E_F and $\boldsymbol{B}/|\boldsymbol{B}|$) and predicts that there will be a singularity in magnetoresistance for the values of $1/B$ which fulfill

$$\frac{1}{B} = n \cdot \frac{|e|}{h} \cdot \frac{1}{A_{min}}, \quad \frac{1}{B} = n \cdot \frac{|e|}{h} \cdot \frac{1}{A_{max}}, \qquad n = 1, 2, \ldots .$$

These two superposed $(1/B)$–periodic structures are called *Shubnikov–de Haas oscillations* and can be observed in an experiment [1],[8].

The Limitations of the SC Approach

The disadvantage of the SC theory is again that it shows no quantitative relation for the conductivity. It only suggests where the singularities of DOS can be. As the superlattice is strongly anisotropic we have no reason to suppose that the conductivity tensor components will all depend on DOS in the same way.

Even from the (almost) classical point of view we may expect that the in–plane component of magnetic field will reduce the tunnelling between two adjacent layers of the sample. Thus for a fixed Fermi level and direction of tilted magnetic field there should be a critical value B_c over which the system will behave as a set of decoupled 2D electron systems. The SC theory cannot predict this transition because regardless of the field strength the Fermi surface cross sections remain the same.

We can thus predict the SC approach failure for strong in–plane field components. As for the experiments this failure (the 3D– to 2D–mode transition) will be indicated by occurence of the Quantum Hall phenomenon (i.e. plateaus in the ϱ_{xy} component of magnetoresistance). We can also expect that the resistance in perpendicular direction (ϱ_{zz}) will rapidly rise.

3.2 Quantum Mechanical Approach

Consider the structure shown at Fig. 3.1. We apply magnetic field $\boldsymbol{B} = (0, B_y, B_z)$ to it and we denote the angle of $\boldsymbol{B}$ to xy–plane as α, i.e. $\cotg \alpha = B_y/B_z$ and we choose $\boldsymbol{A} = (B_y z - B_z y, 0, 0)$ for the vector potential. The Hamiltonian for such a system $\boldsymbol{H} = \frac{1}{2m_*}(\vec{p} - e\vec{A})^2 + V(\boldsymbol{z})$, depends on x thus only via $\boldsymbol{p}_x$. This hints us to make an ansatz $\Psi(x, y, z) = e^{\imath k_x x}\Phi(y, z)$ when solving the stationary–state Schrödinger equation $\boldsymbol{H}|\Psi\rangle = E|\Psi\rangle$. The $2D$ Hamiltonian is then

$$\boldsymbol{H} = \frac{1}{2m_*}(\boldsymbol{p}_y^2 + \boldsymbol{p}_z^2) + \frac{1}{2m_*}(\hbar k_x + |e|(B_y\boldsymbol{z} - B_z\boldsymbol{y}))^2 + V(z)\,. \qquad (3.3)$$

Note that E is independent on k_x for $B_z \neq 0$, because states with different k_x are degenerated and their wavefunctions are only shifted (this can be easily seen from the translational invariance of the kinetic part of $\boldsymbol{H}$). Consequently, it is reasonable to perform the calculation just for one value of k_x, e.g. for $k_x = 0$.

Examining the $\boldsymbol{H}$ we find that it's invariant to translations of the type $(y, z) \mapsto (y + jd_y, z + jd_z)$, $j = 0, 1, -1, 2, \ldots$ where (d_y, d_z) is a vector having the same direction as $\boldsymbol{B}$, in other words $d_y/d_z = B_y/B_z$; local minima of the total potential in $\boldsymbol{H}$ occur at intersection points of lines $z = jd_z$, $j = 0, 1, -1, 2, \ldots$ (corresponding to minima of $V(z)$) and the line $B_y z - B_z y = 0$ (which is the minimum of the parabolic "magnetic" potential). According to the Bloch theorem we can find the eigenstates of $\boldsymbol{H}$ in the form

$$\Phi_{\boldsymbol{k}}(y, z) = \frac{1}{\sqrt{N}} \sum_{j=0}^{N-1} \exp(\imath(k_z jd_z + k_y jd_y))\psi(z - jd_z, y - jd_y) \qquad (3.4)$$

where N is an integer which would be afterwards formally limited to infinity (number of periods of the potential $V(z)$) and $\boldsymbol{k} = (k_y, k_z)$ is a vector of the same direction as $\boldsymbol{B}$, i.e. $k_y/k_z = d_y/d_z = B_y/B_z$. We shall limit ourselves

to the first Brillouin zone, which is determined by $k_z \in (-\pi/d_z, \pi/d_z)$. The function $\psi(y, z)$ is a one–electron state localized in one period of the 2D–potential; note however that this function is also $\boldsymbol{k}$–dependent.

3.2.1   The Approximations

Before we continue with putting the ansatz (3.4) into the Schrödinger equation with the Hamiltonian (3.3) we will make several approximations which will simplify the problem considerably.

1. Separability. $\psi(y, z) = \chi(z)\varphi(y)$. For simpler notation we will use bra and ket vectors $\langle z|\chi_j\rangle = \chi(z - jd_z)$ and $\langle y|\varphi_j\rangle = \chi(y - jd_y)$.

2. Orthogonality of $|\chi_j\rangle$. $\langle \chi_j|\chi_i\rangle = \delta_{ij}$.

3. Tight–binding approximation. $\langle \chi_j|\boldsymbol{H}_z|\chi_i\rangle = t\delta_{j,i\pm1}$. Here we use the notation $\boldsymbol{H}_z = \boldsymbol{p}_z^2/2m + V(\boldsymbol{z})$, i.e. the non–trivial part of $\boldsymbol{H}$ in absence of magnetic field.

4. Setting the zero level of energy (what was however included in the previous point, yet). $\langle \chi_i|\boldsymbol{H}_z|\chi_i\rangle = 0$.

5. Limit on the in–plane field strength. This has two parts: first $B_yz - B_zy$ varies slowly on one period of $V(z)$, or $\langle \chi_j|B_yz - B_zy|\chi_j\rangle = B_yjd_z - B_zy$,

6. and second: $\langle \chi_j|\frac{e^2}{2m_*}(B_yz - B_zy)^2|\chi_i\rangle = 0$ for $i \neq j$.

7. Number of populated states. We assume that the energy spectrum and the number of free electrons in the system is such that only states $|\varphi_j^{(n)}\rangle|\chi_j^{(0)}\rangle$, $n = 0, 1, \ldots$ are populated (i.e. only the ground state of the superlatice in zero magnetic field and an arbitrary state corresponding to the presence of the magnetic field).

The value of the *hopping term t* follows naturally from the exact form of $\chi(z)$. But on the other hand, having specified its value and relying on the listed assumptions we have no other reason why we should be interested in the exact form of $\chi(z)$.

3.2.2   Turning the 2D equation into a 1D equation

We now concentrate on the equation $\boldsymbol{H}|\Phi_{\boldsymbol{k}}\rangle = E|\Phi_{\boldsymbol{k}}\rangle$ with Hamiltonian of the form (3.3) and the ansatz (3.4)

$$|\Phi_{\boldsymbol{k}}\rangle = \frac{1}{\sqrt{N}} \sum_{j=0}^{N-1} \exp(\imath(k_z j d_z + k_y j d_y))|\chi_j\rangle|\varphi_j\rangle\,.$$

We now multiply the Schrödinger equation from the left by

$$\frac{1}{\sqrt{N}} \sum_{j=0}^{N-1} \exp(\imath(k_z j d_z + k_y j d_y))\langle\chi_j|\langle y|\,.$$

By applying the assumptions listed in the previous subsection we arrive (see Appendix C) at an equation which is a sum of N equations (indexed by j) of the type

$$\left\{ \frac{\boldsymbol{p}_y^2}{2m_*} + \frac{1}{2}m_*\omega_\perp^2(\boldsymbol{y} - jd_y)^2 + 2t\cos(\boldsymbol{p}_y d_y/\hbar - k_z d_z - k_y d_y) \right\}|\varphi_j\rangle = E|\varphi_j\rangle\,.$$

$$(3.5)$$

All these summed equations are however equivalent because they can be transformed one to another by substituting $\widehat{y} - j'd_y = y - jd_y$. Due to this we may limit ourselves only to one equation (3.5), let it be the one with $j = 0$. For solving such an equation we choose p_y–representation; we recall $\langle p_y|y|p_y\rangle = \imath\hbar(\mathrm{d}/\mathrm{d}p_y)$ and denote $\langle p_y|\varphi_0\rangle = \varphi(p_y)$. Last, using $d_y/d_z = k_y/k_z = \cot g\,\alpha$ we can write $k_y d_y + k_z d_z = k_z d_z(\cot g^2\,\alpha + 1) \overset{\text{def}}{=} k_z d_z\tau$ and the equation to solve is thus

$$-\frac{1}{2}\hbar^2 m_*\omega_\perp^2\varphi''(p_y) + \left[\frac{p_y^2}{2m_*} + 2t\cos\left(p_y d_y/\hbar - k_z d_z\tau\right)\right]\varphi(p_y) = E(k_z)\varphi(p_y).$$

$$(3.6)$$

3.2.3   Numerical Results

In this section we would like to show only the most important results obtained by solving Eq. 3.6. We will make use of the spectrum only.

It is evident that for each value of k_z we obtain an infinite number of eigenvalues of Eq. 3.6 and thus for k_z going through the first Brillouin zone

we will obtain (Landau) band structure $E_i(k_z)$. As in the previous chapter we will display rather DOS than the band structure itself (Eq. 2.7 shows how to transform $E_i(k_z)$ into DOS).

A typical DOS output for $E_F > 2|t|$ is shown at Fig. 3.2. We can see the overlapping Landau band, each of them having two DOS singularities (at the edges). Both types of singularities (those at the low field edge and and those at the high field edge) are $1/B$–periodic (the periods are not the same) and the periods are in a good agreement with the SC prediction. However, we can see a third DOS maximum at some Landau bands (encircled in the Fig. 3.2). These maxima have no SC analogy and are also $1/B$–periodic.

The conclusion regarding the Fig. 3.2 is that the in–plane component of the magnetic field is not strong enough so that it would cause substantial changes to the system (like the change of dimensionality for instance).
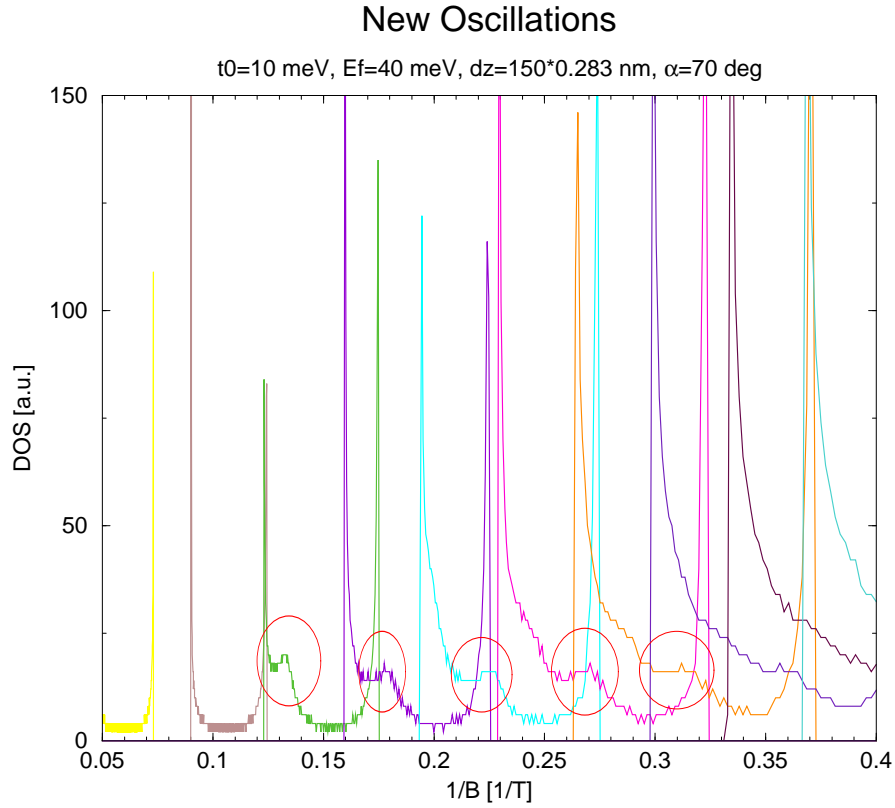

Figure 3.2: DOS at the Fermi level, $E_F > 2|t|$. Note the maxima in circles.

A different situation is shown at Fig. 3.3. We can clearly see the sharp Landau levels for strong magnetic fields and continuous spectrum for low fields. Since sharp Landau levels are typical for 2D behaviour, we conclude that magnetic fields over $B_c \approx 2$ T reduce the dimensionality of the system (i.e. 3D to 2D transition occurs). The SC theory has no means of predicting this phenomenon as it operates with the (extremal) Fermi surface cross sections which are the same for a given Fermi level and field direction regardless of the field strength.
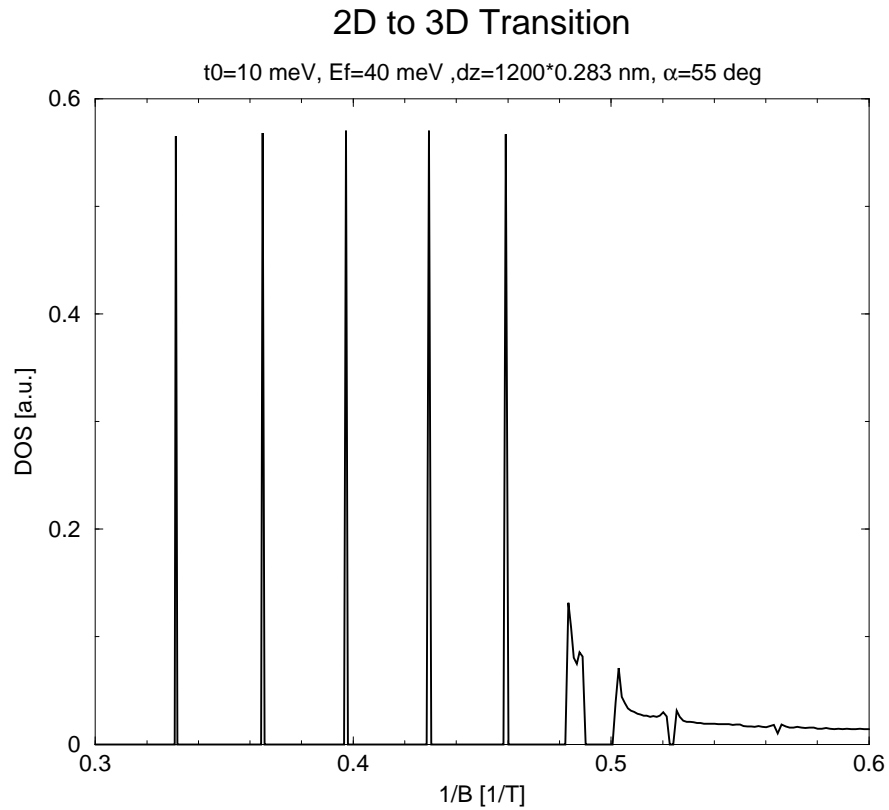
2D to 3D Transition

t0=10 meV, Ef=40 meV ,dz=1200*0.283 nm, α=55 deg

Figure 3.3: DOS at the Fermi level, $E_F > 2|t|$. The system is in the 2D mode for fields over $B_c \approx 2$ T.

Chapter 4

Conclusion

We studied the effect of magnetic field applied to two– and three–dimensional superlattices (SL) on the electric conductivity of the system.

In the case of the *two–dimensional SLs* we applied the standard semi-classical theory first and showed that it cannot explain Shubnikov–de Haas oscillations measured experimentally in magnetoresistance for high concentrations of electrons (*breakdown*), [4]. Next we performed a one electron quantum mechanical calculation of the density of states which was able to reproduce the structure (periodicity) in the experimental data. In the last step we utilized the linear response theory (Kubo formula, [15]) in order to compute directly the conductivity tensor components. These results were in a better agreement with the experiments and thus this direction of improving our model seems to be promising (the first step would be to use a better description of the elastic scattering of electrons on impurities).

There were no such striking experimental results available for the *three–dimensional SLs* which would illustrate the failure of the semiclassical theory. We have however shown by a quantum mechanical calculation of density of states that the dimensionality of the system can change due to the presence of strong in–plane magnetic field. This is again a phenomenon which cannot be predicted by the semiclassical theory.

In general, we showed that the semiclassical theory predicts that the qualitative behaviour (dimensionality) of the system depends on the Fermi level and not on the field strength which turns out not to be true. Moreover, it claims that there is a sharp limit for the Fermi level and the qualitative behaviour of the system changes stepwise when this limit is crossed. This is also not true and it is called a breakdown of the semiclassical theory.

Chapter 5

Appendices

5.1 Appendix A: Density of States in Zero Magnetic Field

If the magnetic field is not present the dispersion relation reads (see Eq. 2.11)

$$E(k_x, k_y) = \frac{\hbar^2 k_x^2}{2m_*} - 2|t| \cos k_y d.$$

So as to calculate the density of states we employ (including spin) the relation (2.5)

$$g(E) = \frac{2}{(2\pi)^2} \int \delta\Big(E - E(k_x, k_y)\Big) \, \mathrm{d}k_x \, \mathrm{d}k_y.$$

Integrating first by k_x we come to an elliptic integral which can be expressed by means of the full elliptic function [7] $K(k) = F(\frac{\pi}{2}, k) = \int_0^{\pi/2} (1 - k^2 \sin^2 \varphi)^{-1/2} \, \mathrm{d}\varphi$:

$$g(E) = \begin{cases} \dfrac{4}{(2\pi)^2} \sqrt{\dfrac{2m_*}{\hbar^2 |t| d^2}} \cdot \dfrac{1}{\sqrt{\gamma}} K\left(1/\sqrt{\gamma}\right) & \text{for } E > 2|t| \text{ or } \gamma > 1, \\[4mm] \dfrac{4}{(2\pi)^2} \sqrt{\dfrac{2m_*}{\hbar^2 |t| d^2}} \cdot K(\sqrt{\gamma}) & \text{for } -2|t| < E < 2|t| \text{ or } 0 < \gamma < 1. \end{cases} \tag{5.1}$$

$$\frac{1 + \beta}{2} = \frac{1 + E/2|t|}{2} = \gamma$$

including the spin degeneracy. We recall that $K(0) = \pi/2$, $K(1) = \infty$ and that the function is monotonous. For $\beta = 1$ the DOS exhibits a logarithmical

singularity. The function plot can be seen at the Fig. 2.8.

Numerically, the prefactor $(2/(2\pi)^2) \cdot (2m_*/(\hbar^2|t|d^2))^{1/2}$ is approximatelly 0.164×10^{11} meV^{-1}cm^{-2} for $2|t| = 1.5$ meV, $d = 15$ nm and m equal to 0.067 times electron vacuum mass (effective mass for GaAs).

5.2 Appendix B: Calculation of Number of States for a Landau Band

It is well known that spectrum of a 2D free electron gas has the form $E_n(k_x) = \hbar\omega(n + \frac{1}{2})$ with $\omega = |e|B/m_*$ and $n = 0, 1, 2, \ldots$ Each of the levels is degenerated so that it contains $|e|B/h$ states per unit area.

We will now show that this property is preserved even if the Landau bands are not flat ($E_n(k_x)$ depends on k_x). We assume that the spectrum consists of continuous bands and only for simplicity also that the bands do not overlap (there are no such k_1, k_2 such that $E_n(k_1) = E_m(k_2)$ for $n \neq m$) and that $E_n(k_x)$ is a monotonous function of k_x on $(0, \frac{1}{2}K)$. We denote the extremes of $E_n(k_x)$ (or the values for $k_x = 0$ and $k_x = \frac{1}{2}K$) by E_{min}, E_{max} and the number of states in this band per one stripe (one period of the superlattice) is then

$$N = \int_{E_{min}}^{E_{max}} g(E) \, dE = \frac{1}{2\pi} \cdot 2 \int_0^{\frac{1}{2}K} \left(k(E)\right)' dE = \frac{K}{2\pi} \, .$$

We have used the inverse function derivative theorem and we have taken into account that $E_n(-k_x) = E_n(k_x)$.

It is easy to see that this idea can be used even if there are more extremes in a Landau band than those in for $k_x = 0$ and $k_x = \pm\frac{1}{2}K$ or if the bands overlap.

The conclusion is that there are $K/(2\pi) = d|e|B/h$ states per one stripe per unit length in the x–direction. The areal concentration of the states is therefore $K/(2\pi d) = |e|B/h$.

5.3 Appendix C: Derivation of Eq. 3.5

We start with the Schrödinger equation $\boldsymbol{H}|\Phi_{\boldsymbol{k}}\rangle = E|\Phi_{\boldsymbol{k}}\rangle$ with

$$\boldsymbol{H} = \frac{1}{2m_*}(\boldsymbol{p}_y^2 + \boldsymbol{p}_z^2) + \frac{1}{2m_*}(\hbar k_x + |e|(B_y\boldsymbol{z} - B_z\boldsymbol{y}))^2 + V(z) \, ,$$

$$|\Phi_{\boldsymbol{k}}\rangle = \frac{1}{\sqrt{N}} \sum_{j=0}^{N-1} \exp(\imath(k_z j d_z + k_y j d_y))|\chi_j\rangle|\varphi_j\rangle \,,$$

and we will use the assumptions 1–7 listed in subsection 3.2.1.

We multiply the Schrödinger equation from the left by

$$\frac{1}{\sqrt{N}} \sum_{j=0}^{N-1} \exp(\imath(k_z j d_z + k_y j d_y))\langle\chi_j|\langle y|$$

and examine the left side first. We are to examine the expression

$$\frac{1}{N} \sum_{j,j'=0}^{N-1} \exp(-\imath(k_z j' d_z + k_y j' d_y))\langle\chi_{j'}|\langle y|\boldsymbol{H}|\varphi_j\rangle|\chi_j\rangle \exp\left(\imath(k_z j d_z + k_y j d_y)\right) .$$

First we focus on terms with $j = j'$ of the result. Let us begin with evaluating $\langle\chi_j|\boldsymbol{H}|\chi_j\rangle$. Due to $\langle\chi_j|\boldsymbol{H}_z|\chi_j\rangle = 0$ (presumption 4) there remain only two terms of $\boldsymbol{H}$: the first of them is

$$\langle\chi_j|\frac{\boldsymbol{p}_y^2}{2m_*}|\chi_j\rangle = \langle\chi_j|\chi_j\rangle\frac{\boldsymbol{p}_y^2}{2m_*} = \frac{\boldsymbol{p}_y^2}{2m_*}$$

and the second can be simplified using the localisation presumption 5:

$$\langle\chi_j|\frac{e^2}{2m_*}(B_z y - B_y z)^2|\chi_j\rangle = \frac{e^2}{2m_*}(B_z y - B_y j d_z)^2 = \frac{m_*\omega_\perp^2}{2}(y - j d_y)^2 \,.$$

At last we introduced the cyclotron frequency $\omega_\perp = eB_z/m_*$ corresponding to the perpendicular component of $\boldsymbol{B}$ and recalled the geometrical relation $d_y/d_z = B_y/B_z$. Now we add the $|\varphi_j\rangle$ vector and we find out that the part of the double sum with $j = j'$ is

$$\frac{1}{N} \sum_{j=0}^{N-1} \frac{m_*\omega_\perp^2}{2}(y - j d_y)^2|\varphi_j\rangle + \frac{\boldsymbol{p}_y^2}{2m_*}|\varphi_j\rangle. \qquad (5.2)$$

Next, we turn to the rest of the terms, i.e. $j \neq j'$. Again, we shall evaluate the three terms of $\langle\chi_{j'}|\boldsymbol{H}|\chi_j\rangle$. Using the presumptions 3, 2 and 6, respectively we obtain

$$\langle\chi_{j'}|\boldsymbol{H}_z|\chi_j\rangle = t\delta_{j,j'\pm1}$$

$$\langle\chi_{j'}|\frac{\boldsymbol{p}_y^2}{2m_*}|\chi_j\rangle = \langle\chi_{j'}|\chi_j\rangle\frac{\boldsymbol{p}_y^2}{2m_*} = 0$$

$$\langle\chi_{j'}|\frac{e^2}{2m_*}(B_y z - B_z y)^2|\chi_j\rangle = 0.$$

Thus from all this terms there remain only

$$\frac{1}{N}\sum_{j=0}^{N-1} t\exp(-\imath(k_z d_z + k_y d_y))|\varphi_{j-1}\rangle + t\exp(\imath(k_z d_z + k_y d_y))|\varphi_{j+1}\rangle. \quad (5.3)$$

We now use the relation $|\varphi_{j-1}\rangle = \exp(\imath\boldsymbol{p}_y d_y/\hbar)|\varphi_j\rangle$, [6], or equivalently in y-representation $\varphi(y+d_y) = \exp(\imath\boldsymbol{p}_y d_y/\hbar)\varphi(y)$. We recall $\cos x = \frac{1}{2}(e^{\imath x} + e^{-\imath x})$ and the expression (5.3) is transformed into

$$\frac{1}{N}\sum_{j=0}^{N-1} 2t\cos(\boldsymbol{p}_y d_y/\hbar - k_z d_z - k_y d_y)|\varphi_j\rangle. \quad (5.4)$$

Last, we take care of the right side of the equation. Again we have a double sum through j, j' to deal with. However, simply using the presumption 2., we realize, that the result is

$$E\cdot\frac{1}{N}\sum_{j=0}^{N-1}|\varphi_j\rangle.$$

By comparing this expression with the sum of (5.2) and (5.4) we have an equation that can be obtained as a sum of N equations of the type

$$\left\{\frac{\boldsymbol{p}_y^2}{2m_*} + \frac{1}{2}m_*\omega_\perp^2(\boldsymbol{y} - jd_y)^2 + 2t\cos(\boldsymbol{p}_y d_y/\hbar - k_z d_z - k_y d_y)\right\}|\varphi_j\rangle = E|\varphi_j\rangle \quad (5.5)$$

Bibliography

[1] N. W. Ashcroft, N. D. Mermin, *Solid State Physics*, Saunders College, Philadelphia 1976

[2] A. Bastin, C. Lewinner, O. Betbeder–Matibet, P. Nozières, *J. Phys. Chem. Solids*, **32**, 1811 (1971)

[3] J. H. Davies: *The Physics of Low Dimensional Semiconductors*, Cambridge university press, 1999

[4] R. A. Deutschmann, W. Wegscheider, M. Rother, M. Bichler, G. Abstreiter, *Physica E*, **6**, 561 (2000)

[5] R. A. Deutschmann, A. Lorke, W. Wegscheider, M. Bichler, G. Abstreiter, *Physica E*, **7**, 294 (2000)

[6] J. Formánek: *Úvod do kvantové teorie*, Academia, Praha 1983

[7] I. S. Gradshteyn, I. M. Ryzhik: *Table of Integrals, Series and Products*, Academic Press, San Diego 1980

[8] O. Jaschinski, *Investigations on the Influence of a Magnetic Field on the Electronic Structure of* $In_{0.53}Ga_{0.47}As/InP$ *Superlattices*, PhD Thesis, Gemeinsame Naturwissenschaftliche Fakultät, Carolo–Wilhelmina Technical University of Braunschweig, Cuvillier Verlag Göttingen, 1998

[9] J. Kolorenč, *Theory of the Hall Effect in Semiconducting Quantum Structures*, Diploma Thesis, Faculty of Mathematics and Physics, Charles University, 2000

[10] R. Kubo, S. I. Miyake, N. Hashitsume, *Solid State Phys.*, **17**, 269 (1965)

[11] A. Manolescu, R. R. Gerhardts, M. Suhrke, U. Rössler: Anisotropic scattering and quantum magnetoresistivities of a periodically modulated 2D electron gas, *Cond. Mat.*, 10.12.2000

[12] G. L. J. A. Rikken et al., Phys. Rev. B **37**, 6181 (1988)

[13] L. Smrčka, *J. Phys. Cond. Mat.*, **2**, 8337 (1990)

[14] R. W. Stark, L. M. Falicov, *Progress in Low Temp. Phys.*, **5**, 235 (1967)

[15] P. Středa, *J. Phys. C: Solid State Phys.*, **15**, 717 (1982)

[16] Ch. Zhang, R. Gerhardts, *Phys. Rev. B*, **41**, 12850 (1990).